

Early Detection of Glaucoma based on Wavelet Domain  
and Design of Experiment using OCT Images



Author

KAINAT ALI

00000275584

Supervisor

DR. MOHSIN ISLAM TIWANA

Co-Supervisor

DR. USMAN AKRAM

DEPARTMENT OF MECHATRONICS ENGINEERING  
COLLEGE OF ELECTRICAL & MECHANICAL ENGINEERING  
NATIONAL UNIVERSITY OF SCIENCES AND TECHNOLOGY  
ISLAMABAD  
AUGUST, 2022

# Early Detection of Glaucoma based on Wavelet Domain and Design of Experiment using OCT Images

Author

KAINAT ALI

00000275584

A thesis submitted in partial fulfillment of the requirements for the degree of  
MS Mechatronics Engineering

Thesis Supervisor:

DR. MOHSIN ISLAM TIWANA

Thesis Supervisor's Signature: \_\_\_\_\_

DEPARTMENT OF MECHATRONICS ENGINEERING  
COLLEGE OF ELECTRICAL & MECHANICAL ENGINEERING  
NATIONAL UNIVERSITY OF SCIENCES AND TECHNOLOGY,  
ISLAMABAD  
AUGUST, 2022

# Declaration

I certify that this research work titled “*Early Detection of Glaucoma based on Wavelet Domain and Design of Experiment using OCT Images*” is my own work. The work has not been presented elsewhere for assessment. The material that has been used from other sources it has been properly acknowledged / referred.

Signature of Student

Kainat Ali

00000275584

2022-NUST-MS-MTS-18

# Language Correctness Certificate

This thesis has been read by an English expert and is free of typing, syntax, semantic, grammatical and spelling mistakes. Thesis is also according to the format given by the university.

Signature of Student

Kainat Ali

00000275584

Signature of Supervisor

Dr. Mohsin Islam Tiwana

# Copyright Statement

- Copyright in text of this thesis rests with the student author. Copies (by any process) either in full, or of extracts, may be made only in accordance with instructions given by the author and lodged in the Library of NUST College of E&ME. Details may be obtained by the Librarian. This page must form part of any such copies made. Further copies (by any process) may not be made without the permission (in writing) of the author.
- The ownership of any intellectual property rights which may be described in this thesis is vested in NUST College of E&ME, subject to any prior agreement to the contrary, and may not be made available for use by third parties without the written permission of the College of E&ME, which will prescribe the terms and conditions of any such agreement.
- Further information on the conditions under which disclosures and exploitation may take place is available from the Library of NUST College of E&ME, Rawalpindi.

# Acknowledgements

I am thankful to my Creator Allah Subhana-Watala who have guided me throughout this work at every step and for every new thought which He setup in my mind to improve it. Indeed, I could have done nothing without His priceless help and guidance. Whosoever helped me throughout the course of my thesis, whether my parents or any other individual was Allah Subhana-Watala will, so indeed none be worthy of praise but one Allah.

I am profusely thankful to my beloved parents who raised me when I was not capable of walking and continued to support me throughout in every department of my life.

I would also like to express special thanks to my dearest supervisor Dr. Mohsin Islam Tiwana for his help throughout my thesis and also for paving a concrete path for our research activity. I can safely say that I haven't learned any other engineering skill and subject in such depth than the one which he has taught. Without his help I wouldn't have been able to complete my thesis. I appreciate his patience and guidance throughout the whole thesis.

I would also like to pay special thanks to Dr. Umar S. Khan for his tremendous support and cooperation. Each time I got stuck in something, he came up with the solution.

I would also like to thank Dr. Usman Akram, for being on my thesis guidance and his work in the glaucoma detection field always acted as torch light in darkness. I also express my special thanks to Ms. Aneeqa for her help. I am also thankful to Dr. Khan (BBH), Prof. Dr. Shakib (RMC) and Dr. Zafar Iqbal for their support and ophthalmological support and cooperation.

Finally, I would like to express my gratitude to all the individuals who have rendered valuable assistance to my study.

*Dedicated to my exceptional parents and adored siblings and  
super supporting husband whose tremendous support and  
cooperation led me to this wonderful accomplishment!*

# Abstract

Nowadays, glaucoma is a progressive, persistent, and chronic eye condition that causes irreparable blindness or visual loss. Globally, around 80 million people will have glaucoma in 2020, and this number is projected to rise to nearly 111 million by 2040. In their early stages, glaucoma is characterized by a lack of symptoms, although it ultimately causes damage to the optic nerve. Review of the scientific literature demonstrates that glaucoma can be managed prior to vision loss or total blindness if it is diagnosed early. In past investigations, the most often employed scanning procedures for glaucoma identification were RNFL analysis and the cup-to-disk ratio. In glaucoma, there is a growing body of evidence supporting the use of statistical analysis optical coherence tomography as a supplemental tool for clinical evaluation and research. In order to diagnose glaucoma early in this study, we apply two main analyses: statistical analysis and identification of retinal layers. We created an image categorization system employing OCT images and discrete wavelet transform. After denoising high-resolution OCT pictures, DWT decomposition is employed to derive statistical characteristics. Statistical characteristics are extracted using the DarkNet-53 neural network. During the second phase, all retinal layers are identified by locating the ROI and using a segmentation technique for each layer. The macular thickness is then computed using the layer borders; for better results, the retinal layers are also identified manually by licensed ophthalmologists. The macular thickness is a statistical characteristic. In the final stage, the outputs of the several blocks are correlated, allowing for the diagnosis of glaucoma stage. In addition, we wanted to introduce the platform for future measurement of macular thickness and the potential utility of macular spectral-domain optical coherence tomography in glaucoma in this study. These procedures will aid experts in the diagnosis and observation of eye diseases by providing them with accurate and precise information regarding the structure of the optic nerve head.

**Key Words:** *Glaucoma, SVM, Deep Learning, OCT, DarkNet-53, DWT, SPSS, Macular Thickness, Vision Loss*



# Table of Contents

<b>Declaration</b> .....	<b>i</b>
<b>Language Correctness Certificate</b> .....	<b>ii</b>
<b>Copyright Statement</b> .....	<b>iii</b>
<b>Acknowledgements</b> .....	<b>iv</b>
<b>Abstract</b> .....	<b>vi</b>
<b>Table of Contents</b> .....	<b>vii</b>
<b>List of Figures</b> .....	<b>ix</b>
<b>List of Tables</b> .....	<b>x</b>
<b>CHAPTER 1: INTRODUCTION</b> .....	<b>1</b>
<b>CHAPTER 2: LITERATURE REVIEW</b> .....	<b>4</b>
2.1    Glaucoma: Eye Condition.....	4
2.2    Glaucoma and its Risk Factors.....	5
2.2.1    Risk Factors.....	8
2.2.2    Image Processing Applications for Glaucoma.....	8
2.2.3    Fundus Images.....	9
2.2.4    OCT Images.....	10
2.2.5    Progression of Glaucoma.....	12
<b>CHAPTER 3: EXPERIMENTATION REVIEW</b> .....	<b>14</b>
3.1    Approaches for Glaucoma Detection.....	14
3.1.1    Introduction to Cup-to-Disc Ratio.....	14
3.1.2    Introduction to Retinal Nerve Fiber.....	16
3.1.3    Machine Learning.....	17
3.1.4    Glaucoma detection through Other Techniques.....	21
3.1.5    Features Extraction and Selection.....	22
3.2    Importance of Early Glaucoma Detection.....	25
<b>CHAPTER 4: METHODOLOGY</b> .....	<b>28</b>
4.1    Pre-Processing Block.....	30
4.1.1    Proceedings of Pre-Processing Block.....	31
4.2    Segmentation Block for Macular Thickness.....	32
4.2.1    Proceedings of Segmentation Block.....	34
4.3    Feature Extraction Block.....	35
4.4    Discrete Wavelet Extraction.....	36
4.5    Statistical Features Extraction.....	37
4.6    Feature Extraction Using DarkNet-53 Model.....	38

4.6.1	Structure of DarkNet-53 Model.....	39
4.6.2	Data Augmentation.....	39
4.6.3	DarkNet-53.....	40
4.7	Feature Selection.....	40
4.8	Correlation based Feature Selection Using SPSS .....	41
4.9	Classification Block.....	42
4.9.1	Proceedings of Classification Block.....	44
<b>CHAPTER 5: RESULTS AND ANALYSIS .....</b>		<b>46</b>
<b>CHAPTER 6: DISCUSSION &amp; ANALYSIS .....</b>		<b>58</b>
<b>CHAPTER 7: CONCLUSION .....</b>		<b>61</b>
<b>CHAPTER 8: FUTURE WORK.....</b>		<b>62</b>
<b>APPENDIX A .....</b>		<b>63</b>
<b>REFERENCES .....</b>		<b>64</b>
<b>COMPLETION CERTIFICATE.....</b>		<b>71</b>

# List of Figures

<b>Figure 2.1:</b> Optic Nerve Head [9].....	5
<b>Figure 2.2:</b> Fundus Images; (a) Glaucoma Eye, (b) Healthy Eye [3] .....	9
<b>Figure 2.3:</b> OCT Images: Glaucoma Eye (left) Healthy Eye (right) [19].....	10
<b>Figure 2.4:</b> OCT Scans .....	11
<b>Figure 2.5:</b> Glaucoma Progression and Development [21] .....	13
<b>Figure 3.1:</b> Cup to Disc Ratio Calculation Concept [23].....	14
<b>Figure 3.2:</b> RNFL in OCT [29] .....	16
<b>Figure 3.3:</b> Types of Machine Learning .....	18
<b>Figure 3.4:</b> Feature Extraction and Selection [40].....	23
<b>Figure 4.1:</b> Block Diagram of Methodology .....	28
<b>Figure 4.2:</b> Block Diagram of Statistical Analysis .....	29
<b>Figure 4.3:</b> Block Diagram of DarkNet-53.....	29
<b>Figure 4.4:</b> Median Filter Working – Edge Preserving and Noise Removal Filter [56].....	31
<b>Figure 4.5:</b> Retinal Layers Segmentation .....	32
<b>Figure 4.6:</b> Flow Chart of Segmentation Block.....	33
<b>Figure 4.7:</b> Flow Chart of Feature Extraction Block .....	35
<b>Figure 4.8:</b> Architecture of DWT and the Filters Level .....	36
<b>Figure 4.9:</b> Structure of DarkNet-53 [57].....	39
<b>Figure 4.10:</b> Classification Block Diagram .....	43
<b>Figure 5.1:</b> OCT Images [59] .....	46
<b>Figure 5.2:</b> Image Histogram .....	47
<b>Figure 5.3:</b> DWT Filter Bands.....	47
<b>Figure 5.4:</b> Automatically Marked Macular Layers .....	49
<b>Figure 5.5:</b> DarkNet-53 Training Fold 1 .....	50
<b>Figure 5.6:</b> Factor Analysis Output I: Total Variance .....	51
<b>Figure 5.7:</b> Factor Analysis Output II: Scree Plot .....	52
<b>Figure 5.8:</b> Factor Analysis Output III: Component Matrix .....	53
<b>Figure 5.9:</b> Factor Analysis Output IV: Rotated Component Matrix .....	53
<b>Figure 5.10:</b> Scatter Plot of the Training Dataset .....	54
<b>Figure 5.11:</b> ROC Curve .....	54
<b>Figure 5.12:</b> Confusion Matrix of SVM linear model .....	55
<b>Figure 5.13:</b> True Positive Results of SVM linear model .....	56
<b>Figure 5.14:</b> Positive Predicted Values of SVM linear model.....	56

# List of Tables

<b>Table 2-1:</b> Glaucoma Types and Causes .....	7
<b>Table 3-1:</b> Glaucoma Detection Methodologies Summary 1 .....	22
<b>Table 3-2:</b> Glaucoma Detection Methodologies Summary 2 .....	26
<b>Table 4-1:</b> Standard and GLCM Features.....	38
<b>Table 5-1:</b> Mean and Standard Deviation of Statistical Features of Glaucomatous Eyes.....	48
<b>Table 5-2:</b> Mean and Std. Deviation of the Retinal layers Path of Glaucomatous Eye .....	49
<b>Table 5-3:</b> Mean and Std. Deviation of the Retinal layers Path of Healthy Eye.....	50

# CHAPTER 1: INTRODUCTION

Glaucoma is a leading cause of blindness in the world. In this disease, increased intraocular pressure and damage to the optic nerve are thought to be the primary causes of permanent vision loss. Glaucoma primarily affects the macular RNFL (mRNFL) and the ganglion cell complex (GCC), which is made up of the thicknesses of the RNFL, GCL, and IPL, in the inner macular retinal layers [1.]. Initially Loss of ganglion cells results from damage to the lamina cribrosa in the macula. Apoptosis, the process by which ganglion cells lose their ties with their axons, occurs first in the affected axons. Because of this, the death or loss of neural impulses is considered the first structural change in the macula.

The symptoms of glaucoma do not show until approximately 63 percent of the nerve has been damaged [2]; they do not appear in the early stages. As intraocular pressure increases, so does the ratio of cup to disc. Neuro-Retinal Rim (NRR) [3] describes the region between the optic curve and the optic disc. The glaucomatous eye is characterized by a high cup-to-disc ratio, often known as cupping, and a decreased NRR area. RNFL analyses are crucial for the early detection of glaucoma because they permit the visual evaluation of NRR. The RNFL became thinner in glaucoma patients, and this validates the inferior thinning of the NRR. ISNT thickness rules apply to RNFL thickness. Thus, the effect of sickness is defined by the ratio of inferior to superior blood vessels in the nasal-temporal area.

Recent research in this subject has demonstrated that there is no preventative treatment for glaucoma, but that early detection, treatment, and management can prevent irreversible blindness [4]. Various tests (such as pachymetry, tonometry, and visual field tests) are used to identify glaucoma. Recently, imaging techniques such as fundus photography and optical coherence tomography (OCT) have found broad usage in the diagnosis and management of glaucoma. Typically, structural abnormalities precede functional changes in glaucoma. Consequently, the early diagnosis of glaucoma depends

on the detection of these structural abnormalities. Measurements of circumpapillary RNFL (cpRNFL) and GCC thickness have a strong potential to detect early glaucoma. The significance of spectral-domain OCT for the early identification of glaucoma is the primary focus of current research. Furthermore, machine learning techniques have been utilised to automatically identify glaucoma. Features retrieved from segmented OCT volumes using machine learning techniques like KNN, SVM and RF; and deep learning techniques like CNN [5]. The thickness of the peripapillary RNFL and the thickness of the macular GCIPL are two well-established metrics used by classical machine learning algorithms to discriminate between healthy and glaucomatous eyes. An important yet out-of-date approach for determining glaucoma's presence is the computed CDR.

Diagnosing glaucoma at an earlier stage than is now possible could be facilitated by the detection of structural changes before the onset of clinically detectable illness. Using low-coherence interferometry, optical coherence tomography (OCT) produces cross-sectional pictures of ocular tissue with excellent resolution. OCT has been demonstrated to be a non-contact, non-invasive imaging approach for the anterior and posterior eye parts [6]. Using the OCT model technique, numerous retinal problems, including glaucoma, are evaluated and observed. It also allows for early detection and diagnosis of glaucoma progression.

When it comes to eye disease, myopia has long been recognised as an important risk factor. As the frequency of myopia continues to rise, it is imperative to be able to identify and treat glaucoma in this group. As a result, structural changes linked to glaucoma in myopic eyes, especially those that are highly myopic, are difficult to diagnose. It is hard to distinguish RNFL flaws in red colour base-free photography in eyes with extreme myopia. OCT scanning can also be hindered if the optic disc is tilted or if the PPA is large enough to obscure the Neuroretinal rim constriction.

The necessity for an early glaucoma detection model has arisen. The primary purpose of this project is to construct a highly accurate statistical data-based detection and prediction model for early glaucoma. For effective glaucoma analysis, both retinal

fundus image and OCT image image processing techniques are utilised. The key contributions of our study are as follows:

- The most important contribution is the incorporation of macular thickness relationship with other glaucoma indicators. This can eventually lead to the identification of glaucoma at a very early stage.
- Our proposed system increases glaucoma recognition ability as well as the system's computing capacity.
- The system's solid framework is established by utilizing the most important characteristics of normal and glaucomatous eyes.
- On the supplied OCT picture dataset from three separate ophthalmologists, exceptional performance assessments have been observed.

The remainder of the document is formatted as follows:

- Section 2 discusses related work
- While Section 3 explores the proposed offered strategy and method
- Section 4 describes the study and outcomes, as well as the database and evaluation measures employed
- Section 5 includes the conclusion and proposed next work

# CHAPTER 2: LITERATURE REVIEW

## 2.1 Glaucoma: Eye Condition

The chronic and deteriorating optic neuropathy and abnormalities of the visual field that are associated with glaucoma can have a variety of etiologies [2]. Glaucoma is a condition in which the visual nerve is destroyed by an increase in intraocular pressure [3]. Aqueous humour is produced by the ciliary body and enters the trabecular mesh through the pupil. Trabecular mesh drainage and aqueous humour production should proceed at the same pace. A person with glaucoma will experience symptoms if the ocular elevation is around 20 and 24 mmHg, which is the normal range. Glaucoma is diagnosed when the intraocular pressure surpasses 24 mmHg. When the eye's anterior chamber pressure rises, so does the posterior chamber pressure, which in turn damages the optic nerve head's fibres further [9]. Early symptoms of glaucoma are often unnoticed since it is a neuropathy that progresses slowly. The axons of ganglion cells die as a result of glaucoma, leading in permanent visual loss. To give you some idea of how densely packed an optic nerve is, consider looking at Figure 1. Cupping is the medical term for this ailment. Thinner nerve fibres lead to a larger cup because the axon layer is lost. What's perhaps more worrisome is that permanent blindness occurs before any visible loss of vision field. The RNFL degradation in 60% of individuals occurred at least six years prior to the onset of visual deficits. Peripheral vision loss is difficult for patients to detect in the early stages of glaucoma. Pictured in Figure 1 are the optical fields of healthy people and glaucoma sufferers at different stages of the disease. Glaucoma's early phases need that the RNFL loss be thoroughly evaluated. Glaucoma is more common in certain persons than in others. Nearsighted or myopic adults over the age of 40 who are diabetic and have narrow angles are included in this group. They are also long-term steroids or cortisone users, have high intraocular pressure, and inflamed optic nerves [10,11].



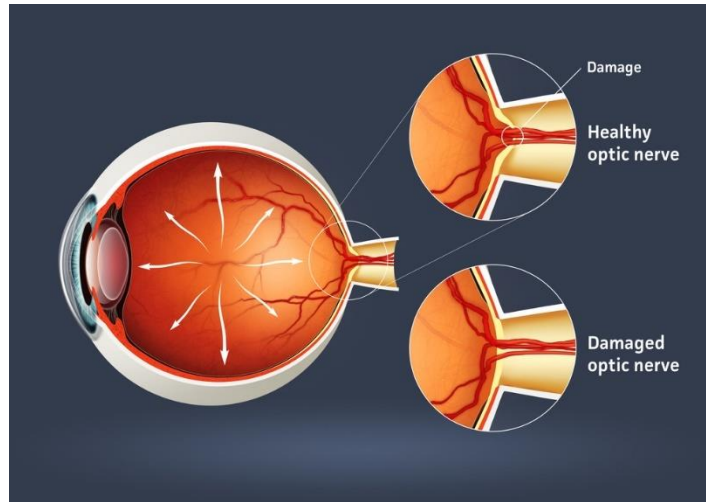


**Figure 2.1:** Optic Nerve Head [9]

## **2.2 Glaucoma and its Risk Factors**

Glaucoma is a debilitating eye disease that can never be cured. Damage to the optic nerve, which is necessary for clear vision, is the result of a group of eye illnesses. Intraocular pressure is generally elevated following this injury, however it is usually only noticeable in its latter stages. Among people over 60, glaucoma is the leading cause of blindness. Anyone can get it, although the elderly are more at risk. Symptoms of glaucoma in many forms are not present. You may not notice a change in your vision until the problem has progressed since the effect is so subtle. Because the loss of vision caused by glaucoma cannot be reversed, regular eye exams with the measurement of your eye pressure are essential for early detection and treatment. If glaucoma is diagnosed early, vision loss can be postponed or even prevented. Depending on the type and stage of disease, the common symptoms of glaucoma might vary. Optic nerve damage results in glaucoma. Blind spots develop in your range of vision when the health of this nerve deteriorates over time. For unknown causes, higher intraocular pressure is frequently seen in patients with this nerve damage. Elevated intraocular pressure is caused by a buildup of a fluid (aqueous humour) in the eye's interior. At the iris-cornea intersection, the trabecular meshwork empties this internal fluid. Increasing ocular pressure occurs when fluid production is excessive or when the septic tank is malfunctioning.

There are a variety of glaucoma forms, including:

- **Open-Angle Glaucoma**

Open-angle glaucoma is the most prevalent kind of glaucoma. However, the trabecular meshwork is partially obstructed. This produces a progressive increase in intraocular pressure. This stress is harmful to the visual nerve. It occurs so gradually that vision loss may occur before you realise there is a problem.

- **Angle-Closure Glaucoma**

Angle-closure glaucoma can occur when the iris pushes forward and decreases or inhibits the drainage angle created by the corneal and the iris. Closed-angle glaucoma is the medical term for this ailment. This results in a rise in eye pressure because fluid cannot move normally within the eye. Angle-closure glaucoma is more likely to occur in those who have narrowed drainage angles during the course of their lives. It is possible for angle-closure glaucoma to appear suddenly or gradually over time. A medical emergency, acute angle-closure glaucoma must be treated immediately.

- **Normal-Tension Glaucoma**

Even if your corneal thickness is within the normal range, the optic nerve is damaged in normal-tension glaucoma. This is a mystery, and no one knows why. Your optic nerve may be more sensitive or receive less blood supply, depending on your circumstances. It's possible that atherosclerosis, the buildup of fatty deposit (plaque) in the arteries, is to blame for this reduced blood flow.

- **Children's Glaucoma**

Glaucoma is a condition that can develop in young children and newborns. It is possible for a person to be born with it or for it to develop over the first few years of life. The damage to the optic nerve could have been caused by clogs in the drainage system or by an underlying medical condition.

- **Pigmentary Glaucoma**

Pigment granule from the iris build up in the drainages of patients with pigmentary glaucoma, which slows or halts the outflow of fluids from the eye. This condition is known as pigmentary glaucoma. Jogging and other activities can occasionally cause pigment granules to get dispersed on the mucous membrane, which can result in transient rises in intraocular pressure.

**Table 2-1:** Glaucoma Types and Causes

<b>Glaucoma Types</b>	<b>Causes of Disease</b>
Acute Glaucoma	A sudden increase in IOP caused by the excessive propagation of hydrous humour over the course of hours.
Pigmentary Glaucoma	Nearby glimpse eye is similarly concaved to the iris, causing hydrous humour to splatter on trabecular meshwork, culminating in its closure.
Trauma related Glaucoma	Due to traumas, accidents, or inflammatory disorders, the ocular drainage canal may undergo morphological alterations.
Uveitic Glaucoma	Glaucoma weakens up to 20% of sufferers and has several causes of ocular inflammation (uveitis). It is common for some of these disorders to affect just one eye. Those that can harm both eyes are known as asymmetrical.
Congenital Glaucoma	Typically, infants are affected by this kind of glaucoma. Congenital Glaucoma is caused when a pregnant woman's unborn child's eye drainage canal system fails to develop properly.

Pseudo exfoliative glaucoma	In order to develop pseudo exfoliative glaucoma, the external layer of the eye's lens must be peeled away. In the angle between both the iris and cornea, this ash-like substance collects and destroys the entire eye system.
Neovascular glaucoma	This kind of glaucoma is linked to diabetes. This type of glaucoma is difficult to treat because clogged blood vessels allow eye fluid to leave the drainage canals.

### 2.2.1 Risk Factors

Glaucoma is a chronic disease with many underlying risks. The risks are clinical as well as inter related to the other eye diseases. Glaucoma has the following risk factors:

- One having high intraocular pressure (intraocular pressure);
- Over the age of 60;
- Locality like black, Asian, or Hispanic;
- Family history of glaucoma;
- Certain medical conditions, including diabetes, heart disease, high blood pressure, and sickle cell anemia;
- Family history of glaucoma
- Centrally thin corneas
- Extreme nearsightedness or farsightedness
- Eye damage or some forms of eye surgery
- Long-term use of corticosteroid drugs, particularly eyedrops

### 2.2.2 Image Processing Applications for Glaucoma

Research into the different applications of medical image segmentation has been ongoing for the last few decades. One of the key goals of medical image analysis research [9,10] is to assist clinicians in the detection of diseases based on visual information.

Almost all glaucoma tests are time-consuming, expensive, and require specialized knowledge. Recently, the devices used by ophthalmologists such as Heidelberg Retinal Tomography (HRT), SD-Spectralis (Heidelberg Engineering, Dossenheim, Germany), SD-the Cirrus (Carl Zeiss Meditec, Dublin, CA), SD-the RTV (Optovue Inc., Fremont, CA), and Swept source optical coherence tomography (SS-OCT) all operate on similar principles but differ in diagnostic ability, acquisition speed, and Color fundus photography and OCT are the two primary modalities now available to clinicians for assessing the anatomy of the ONH.

### 2.2.3 Fundus Images

Combining color fundus imaging with image processing algorithms has assisted in the diagnosis and grading of eye disorders [13,14]. Retinal fundus photography is commonly obtained for the diagnosis and documentation of many eye diseases and is a suitable screening exam due to its simplicity and low cost. The availability of digital fundus cameras in primary care settings and their widespread use in eye screening programs explain the interest in glaucoma screening with this picture modality. Nevertheless, the subjective interpretation of color fundus pictures for the identification of glaucomatous symptoms is a difficult undertaking requiring years of training and experience [15]. The sample fundus image can be seen in figure 2.2

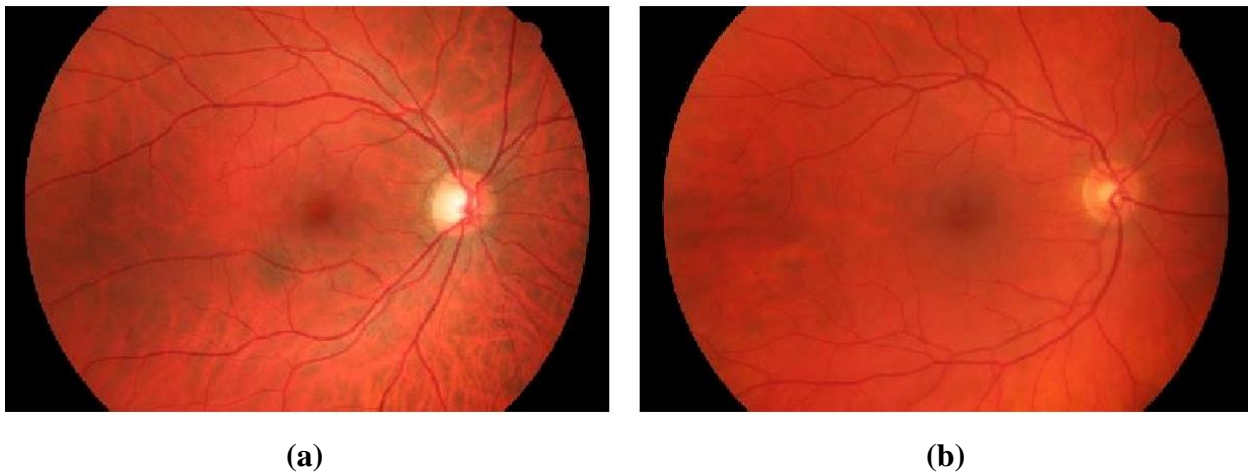


**Figure 2.2:** Fundus Images; (a) Glaucoma Eye, (b) Healthy Eye [3]

Recently, several DL studies have also used fundus images to predict the presence of structural defects [16] (e.g. peripapillary atrophy) with varying accuracies (AUCs ranging from 0.66 to 0.97) or to predict ONH structural parameters (e.g. RNFL thickness) that could not be directly measured from fundus images. Since glaucoma is a "3D illness" with depth-resolved structural alterations, it might be claimed that fundus imaging will never be able to provide the same level of accuracy as 3D imaging modalities such as OCT [17].

#### 2.2.4 OCT Images

At the moment, wavelet-based technology is implemented into each and every one of the OCT devices. While the operating concept of time domain OCT is associated with the delay in the time of light's reflection, the real variable in spectral domain OCT is the change in the guided wavelength. This is because time domain OCT measures the delay in the time of light's reflection. Good axial resolution, minimum eye movement interference, and low artefacts are among the important features that set these clinically verified devices apart from one another.

To this day, the axial resolution of spectral domain OCT devices has reached up to 3 microns, and it is fair to refer to these devices as OCTs with extremely fast speeds and extremely high resolutions because they possess both of these characteristics [18,19].

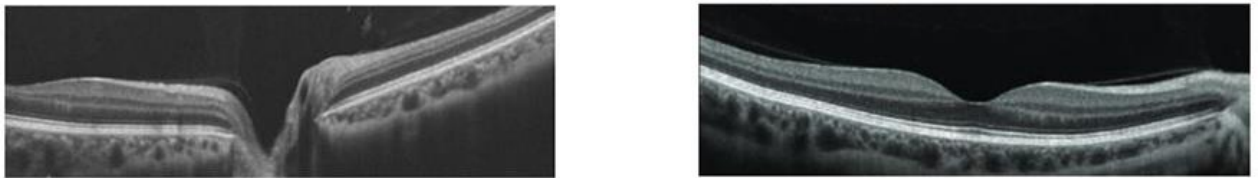


**Figure 2.3:** OCT Images: Glaucoma Eye (left) Healthy Eye (right) [19]

The optical coherence tomography (OCT) method of acquiring cross-sectional pictures of anatomical areas such as the retina is non-invasive. It makes use of the principles of reduced interferometry, and the essentials of image restoration are analogous to ultrasound imaging (pulse and echo). Ultrasonic imaging creates an A-scan reflection profile with depth information based on the position of internal layers [20]. A

cross-sectional picture known as a B-scan is formed once axial stacking of B-scans and lateral integration of A-scans, both of which exhibit three-dimensional representations [21], have been completed. OCT can provide information that can be utilised to identify visual issues such as diabetic retinopathy, and it is frequently used for the monitoring of glaucoma due to the fact that it needs less time, precision, and expert expertise than other diagnostic methods. OCT can diagnose preperimetric myopia with a high degree of specificity and sensitivity since it concentrates on the optic disc and macular area of the eye. It provides measures that are reproducible for the RNFL, ONH, and inner macula. The assessment of the inner macula thickness with SD-OCT is an alternate method that can be useful for tracking the progression of glaucoma. When analysing the course of glaucoma, it is necessary to take into consideration age-related changes, the severity of the illness, and the signal-to-noise ratio of Image data [22]. OCT pictures, also known as scans or sites, might be one of two different varieties, as seen in figure 2.4:

- Macular OCT Images (Around the fovea)
- Optic Nerve OCT Images (Around the optic nerve head)

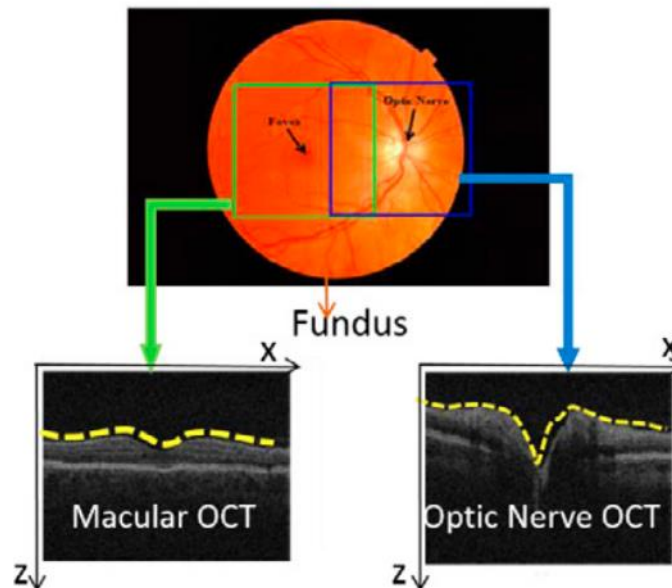


**Figure 2.4:** OCT Scans

### **2.2.5 Progression of Glaucoma**

Glaucoma is a set of eye illnesses characterized by optic nerve damage typically caused by an extremely high intraocular pressure (IOP). If left untreated, this elevated intraocular pressure can damage the optic nerve, leading in progressive, permanent vision loss, beginning with imperceptible blind patches at the periphery of the field of vision, moving to tunnel vision, and ultimately to total blindness. Glaucoma is often regarded as a slow-progressing eye condition. In the most prevalent form of glaucoma, primary open-angle glaucoma, retinal cell loss begins fairly gradually. In several years, glaucoma can lead to blindness if left untreated.

Typically, early diagnosis and treatment result in high success and preservation of vision. The goal of glaucoma treatment is to limit the disease's progression and prevent it from impairing your quality of life. Medication, surgery, or laser surgery may be used to treat a condition. Typically, eye drops or medications can moderate glaucoma, but they cannot cure it. Some medications are intended to reduce intraocular pressure by reducing the flow of fluid into the eye, whilst others aid in fluid drainage. Fluid drainage surgery and laser surgery are now frequently utilised for the same reason.

The chance of developing glaucoma grows considerably with age, but it can affect people of any age, including newborns and fetuses. To preserve good vision and eye health, it is essential to have your eyes examined periodically. Early detection of glaucoma is essential for stopping the disease's progression and averting blindness.



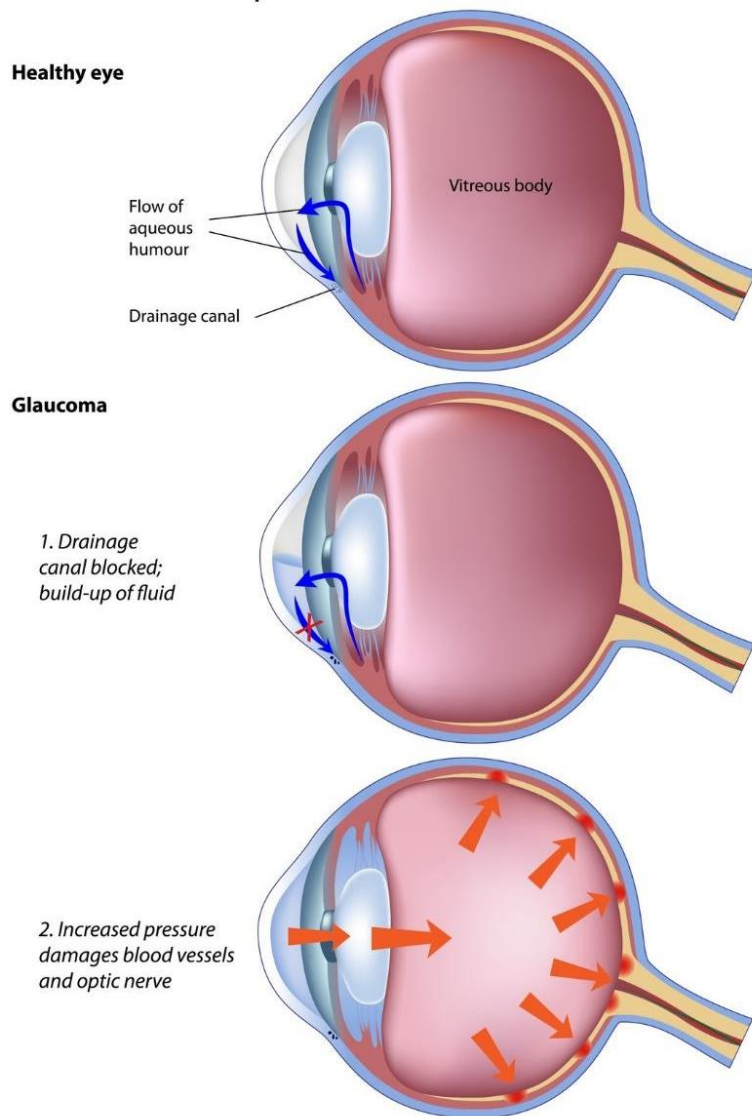


**Figure 2.5:** Glaucoma Progression and Development [21]

# CHAPTER 3: EXPERIMENTATION

## REVIEW

### 3.1 Approaches for Glaucoma Detection

#### 3.1.1 Introduction to Cup-to-Disc Ratio

Examining the Neuroretinal rim (NRR) and noticing aberrant measurements of the inferior, superior, nasal, and temporal rims is referred to as optic disc thinning. The "ISNT" rule is useful for memorizing the order of thickest to thinnest rims in a healthy disc in order to calculate the NRR. Evaluation of glaucoma begins with the cup-to-disk (C/D) ratio. However, this single measurement might be deceiving if not assessed in conjunction with other characteristics, such as overall disc size, location of disc thinning, alterations in vasculature, color changes, peripapillary atrophy, and asymmetry between the eyes.

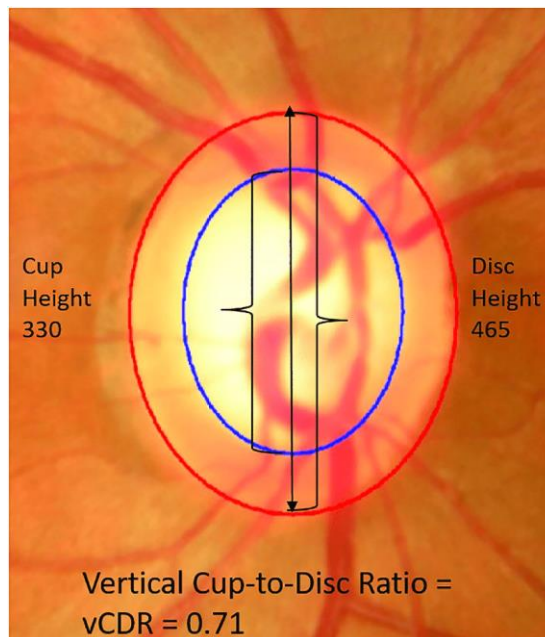


**Figure 3.1:** Cup to Disc Ratio Calculation Concept [23]

### 3.1.1.1 Glaucoma detection through Cup-to-Disc Ratio

Calculating the Cup-to-disc ratio is the most conventional method for detecting glaucoma (CDR). CDR is a key symptom of glaucoma, and detecting and correctly segmenting the optic disc is a tough and critical step. The concept of finding the CDR can be seen in figure 2.5. Shekhar S. [23] utilised a method in which the optic disc is automatically segmented by means of morphological processing and circular Hough transform. As glaucoma progresses, it causes variations in the form, color, and depth of the optic disc, which can also be used for identifying purposes. Dua S. [24] employed texture features, such as wavelet-based energy features, to detect glaucoma in photos. CDR segmentation was conducted for glaucoma detection by segmenting the disc and cup regions, from which the CDR was calculated<sup>14</sup>. For CDR computation, the vertical disc and cup diameters were measured using fundus pictures. If the CDR is  $>0.3$ , glaucoma is indicated. In addition, some research has been conducted on the automated segmentation of the optic disc and optic cup using fundus pictures.

Aquino et al. [26] also employed morphological processes, edge detection, and feature extraction for the detection of the optical disc boundary. For the identification of optic cup, the Vessel Kinking technique [27] border with altering multi-scale window interval to probe along the vessels has been utilised. Even if several image processing algorithms have been developed, there is still a need for a more efficient and less complicated method that is independent of image quality for glaucoma screening [28]. For successful segmentation of the optic disc and cup, an iterative clustering approach is utilised, and the histogram-derived characteristics are considered for pixel classification. The disc and cup regions are segmented using super pixel classification.

R. Nithya [25] proposed the investigation in which fundus and OCT images of the same patient are analyzed. In order to improve segmentation techniques, the CDR was determined by analyzing both types of images with several algorithms, namely the region growth algorithm, the hill climbing methodology, and the fuzzy C-mean clustering algorithm. The cup to disc ratio (CDR) is derived from both analyses, and the results are compared to clinical values. The experimental findings indicate that the performance

error in OCT image analysis is less than in fundus image analysis. The identification success rate for glaucoma in a collection of fundus pictures was 88.5%. According to the authors, future research should employ a larger collection of fundus photos to achieve an accurate evaluation. [29].

### 3.1.2 Introduction to Retinal Nerve Fiber

OCT devices calculate RNFL thickness as the distance between the internal limiting membrane and the outside surface of the NFL. Because RNFL thickness fluctuates with distance from the optic nerve's center, most machines utilize a circle with a predefined diameter (typically between 3.41 and 3.47 mm) as the reference point for calculating RNFL thickness. One of the reasons why measurements of the RNFL cannot be compared between machines is because different machines utilize circles with varied widths around the optic nerve head's center. RNFL is seen in Figure 2.7.

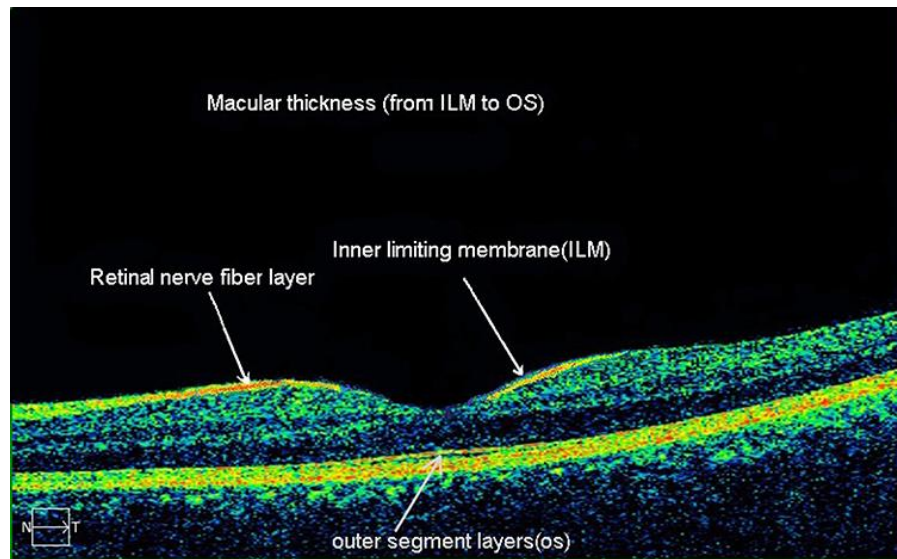


**Figure 3.2:** RNFL in OCT [29]

#### 3.1.2.1 Glaucoma detection through Retinal Nerve Fiber

An algorithm for segmenting retinal layers in OCT pictures has been suggested. The technique makes use of gradient information including local canny edge detection and global intensity gradient [30]. For determining the thickness of the Retinal Nerve

Fiber Layer (RNFL) and the macular volume from OCT images that can be seen in figure 2.6, variance analysis and Bonferroni's correction are utilised. Using the aforementioned factors, three classifications are determined: healthy, early-stage glaucoma, and advanced glaucoma.

With an OCT prototype, previous research has demonstrated the reliability of retinal thickness measurements in normal eyes and glaucomatous eyes. At sites 500 mm or beyond from the fixation point, the coefficient of variation in retinal thickness was less than 10 percent on average in one study. This early, noncommercial OCT prototype displayed adequate repeatability in both normal and glaucomatous eyes, as reported by Schuman et al. The intrasubject standard deviations for a scan with a 3.4-mm diameter and internal fixation were 13 and 21 mm for normal and glaucomatous eyes, respectively. This previous exploratory version required a significantly longer acquisition time (2.5 seconds as opposed to 1 second) and was equipped with a fiberoptic delivery system attached to a slit light. Using retinal fundus images and OCT images of the same eyes, we demonstrate an effective glaucoma detection technique. Comparing K-means clustering with Otsu thresholding for structural features analysis. The thickness of the Retinal Nerve Fibre Layer (RNFL) is estimated from the OCT picture. Support Vector Machine (SVM) with many classes is utilised to classify both datasets. The work is applied to data acquired from an eye hospital including glaucomatous, non-glaucomatous, and glaucoma suspect patients. The results indicate 90 percent accuracy for fundus pictures and 92 percent accuracy for OCT images. The identification stage of glaucoma is attained by comparing the results of retinal fundus images and OCT images.

### **3.1.3 Machine Learning**

When it comes to solving problems that can't be solved using simply numerical approaches, Machine Learning is the answer. Machine learning is a key area of Artificial Intelligence research (AI). In the absence of explicit coding, ML systems learn by doing, just like humans do. These apps detect and classify, grow, adapt, and evolve when they are exposed to fresh data. To put it another way, machine learning is the process of computers finding useful information on their own. Instead, they use algorithms that can learn from data in an iterative fashion. It is this ability to adapt to new information that is

at the heart of machine learning. Apps use "pattern recognition" and "learn" from previous computations and transactions to provide reliable, well-informed outcomes.

### 3.1.3.1 Working of ML

The first step in the Machine Learning process is to feed the selected algorithm with some training data. Training data are data used in the construction of the final algorithm for machine learning, and can consist either as known or unknown data. The training data input type has an effect on the algorithm, which is a topic that will be explored in further depth in the following paragraphs. In order to ensure that the deep learning system is operating correctly, fresh input data is continuously sent to it. The forecast and the outcomes are then contrasted with one another. The algorithm is trained up until the data analyst reaches the outcome that is sought if the prediction and the results do not coincide.

### 3.1.3.2 Types of Machine Learning

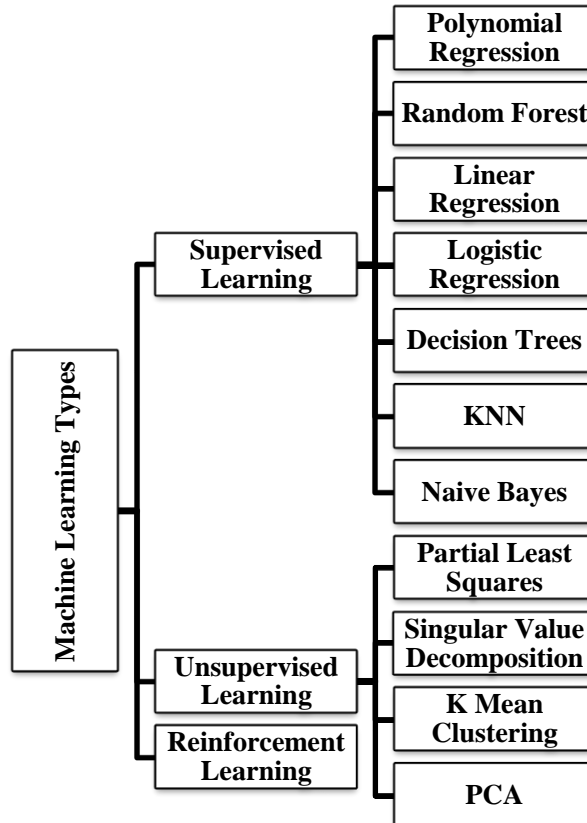


**Figure 3.3:** Types of Machine Learning

### **3.1.3.2.1 Supervised Learning**

In the process of supervised learning, the computer receives its instructions from outside observations. The operator provides the machine learning technique with a dataset that includes the required inputs, and it is the responsibility of the system to figure out how to access those inputs. Even though the operators is aware of the appropriate answers to the issue, the algorithm is able to discern data patterns, learn from observations, and make predictions. The algorithm generates predictions, which are then modified by the operator; this cycle is continued until the algorithm achieves a high level of accuracy and performance.

### **3.1.3.2.2 Unsupervised Learning**

Unsupervised learning is an area of a machine utilising unredacted or unidentified data and enabling the algorithm to act on the information without supervision. The purpose of this application is for the machine to classify data that has not been sorted based on the similarities, patterns, and variances without receiving any prior data training. In contrast to reinforcement methods, unsupervised learning does not include the provision of an instructor. As a result, the system will not be instructed. As a consequence of this, the machine is the only one capable of unearthing the concealed structure inside the unsupervised learning on its own.

### **3.1.3.2.3 Reinforcement Learning**

The primary focus of reinforcement learning is on organised learning processes, such as those in which an algorithms for deep learning is provided with a predetermined set of actions, variables, and end values. After the criteria have been specified, the algorithm for machine learning will make an effort to investigate a wide range of alternatives and opportunities while continuously monitoring and analysing the results in order to locate the most suitable answer. A computer is taught, through the process of reinforcement learning, how to understand through trial - and - error. It starts modifying its approach as a reaction to the scenario in order to acquire the biggest feasible result based on its previous experiences. This is done in order to get the best possible result.

### 3.1.3.3 Glaucoma detection through Machine Learning (ML)

A clinically useful indication of glaucoma is the RNFL and the GCIPL. Automatic detection of glaucoma has recently been made possible with the application of machine learning algorithms. Classical machine learning algorithms, such as KNN, SVM, RF, and others, may be applied to features derived from segmented OCT volumes; deep learning methods, such as Deep Neural Networks, can also be employed (CNN). RNFL average thickness, four quadrants, and 12 clock hours, as well as visual field test parameters such as mean and standard deviation (MD), pattern standard deviation (PSD), and glaucoma hemifield test (GHT)—were used to train 10 classical machine learning methods [31] on a dataset containing 62 patients with glaucoma and 48 healthy individuals. Using the Random Forest [10] classifier, we were able to get the highest AUC of 0.946%. Interestingly, an AUC of 0.915 was achieved by only one feature (PSD), which is not statistically significant from the greatest AUC of 0.946 when all features are considered ( $p = 0.37$ ).

A comparable research by Kim, Y. et al. [32] included 297 glaucoma eyes and 202 normal eyes as a bigger sample. Four ml algorithms (C5.0, Random Forest (RF), Support Vector Machine (SVM), k-Nearest Neighbor (KNN)) were trained to detect glaucoma using age, intraocular pressure (IOP), mean RNFL thickness, corneal thickness, MD, GHT scores, and PSD. C5.0 had the greatest AUC of 0.979 percent, followed by RF at 0.976 percent. [33] An adaptive neurofuzzy inference system (ANFIS) is created for glaucoma diagnosis from OCT images of the stratus. As feature vectors, the RNFL and ONH are analysed to use an orthogonal array approach. Back-propagation gradient descent and least squares techniques are used to train ANFIS using the specified features. OCT images are used to perform a glaucoma thickness assessment based on the image registration [34].



### 3.1.4 Glaucoma detection through Other Techniques

Peripapillary atrophy, which is classified into two categories, a-zone and b-zone, can indicate glaucoma. [35]. According to the scientists, the B-zone category is connected with the progression of glaucoma, and glaucomatous eyes with PPA exhibit faster retinal nerve thinning than normal eyes. In the suggested technique, OCT B scan pictures were utilised to determine optic disc diameters. In this study, 115 participants were investigated, and Peripapillary atrophy was used to classify the presence of glaucoma. Peripapillary atrophy is varied and considered a very progressive morphological diagnostic for open-angle glaucoma [36], according to the authors. Glaucomatous eyes have significant peripapillary atrophy. For measuring peripapillary atrophy, confocal scanning laser tomography and automated static threshold perimetry are employed [51]. A total of 102 eye samples were examined, and the entropy was separated into two zones. The first zone was central with large, visible vessels, while the second was periphery with hyperpigmentation. The scientists found that peripapillary atrophy is related with injury to the optic nerve, the leading cause of glaucoma [37].

By determining the minimal distance that exists between the Bruch membranes opening (BMO) and the interior limiting membrane (ILM), the SD-OCT software developed by Heidelberg Engineering, Inc. in conjunction with an anatomical positioning system (APS) accurately detects the neuroretinal rim tissue (ILM). This BMO–minimum rim width (MRW) delivers the most accurate assessment possible of the geometry of the neuroretinal rim [38]. Recent studies have shown that the BMO–MRW method of diagnosing glaucoma gives a more precise diagnosis of the condition and a higher association with functional metrics [39]. It has been pointed out by a variety of authors [40] that BMO–MRW can be helpful in the diagnosis of glaucoma in eyes that have intermediate myopia or short optic discs. BMO–MRW revealed good intraday reproducibility and independence from fluctuations in intraocular pressure (IOP), which are features that are similar to those of the RNFL thickness [40].

**Table 3-1: Glaucoma Detection Methodologies Summary 1**

<b>Study by</b>	<b>Methodology</b>	<b>Dataset</b>	<b>Result</b>
Fathima C S., Subhija E N. [2]	KNN RNFL Methodology based on OCT & Fundus images	OCT and Fundus Malabar eye care hospital, Thrissur, Kerala	90% accuracy for fundus and 92% for OCT images.
Gopi et.al. [41]	A fuzzy C-Means clustering technique is used to segment optic disk and Otsu thresholding method for the optic cup segmentation	Fundus Venu Eye Institute & Research Centre	Accuracy of 97.67% and sensitivity is about 98%.
Ferrandez et al. [42]	Bruch membrane opening–minimum rim width (BMO–MRW) assessment	136 individuals, 68 mild POAG patients and 68 healthy control subjects	AUCs 0.875 0.879 global RNFL thickness
Nithya. et al. [43]	Analysis of Segmentation Algorithms in OCT & Fundus	Fundus and OCT images Dr. Agarwal Eye Hospital, Chennai	Glaucoma detection is done more effectively using OCT image analysis.
Dutta et al. [44]	Adaptive Threshold based Technique in Fundus Image	Fundus Images	90% Accuracy
Liu. J et al. [45]	Superpixel classification based optic disc and optic cup segmentation for glaucoma screening	Fundus Images 650 images	AUC of 0.800 and 0.822 in 2 datasets
Omodaka et al. [46]	Machine Learning	208 glaucoma eyes 149 healthy eyes	AUC 0.963

### 3.1.5 Features Extraction and Selection

The technique of feature extraction is a type of dimensionality reduction that organises an initial set of original data into subsets that are easier to manage for the purposes of processing. Massive data sets are defined by an enormous number of variables, the processing of which requires a significant amount of computational resources. The term "feature extraction" refers to methods that select and/or combine variables into features. As a result, the amount of data that needs to be processed is reduced, but the original data set is still exhaustively and precisely described. Feature extraction is helpful when there is a requirement to lessen the amounts of resources necessary for process while at the same time preventing the loss of information that is

essential or relevant. In addition, the extraction of features has the potential to lessen the amount of data that is redundant for a specific study. In addition, the amount of data that is used and the efforts made by the machine to generate variable combinations (features) both contribute to an improvement in the speed of the learning and generalization stages of machine learning. A graphic taken from analyticsvidhya's article provides a crystal-clear illustration of the difference between feature extraction (figure 2.9).

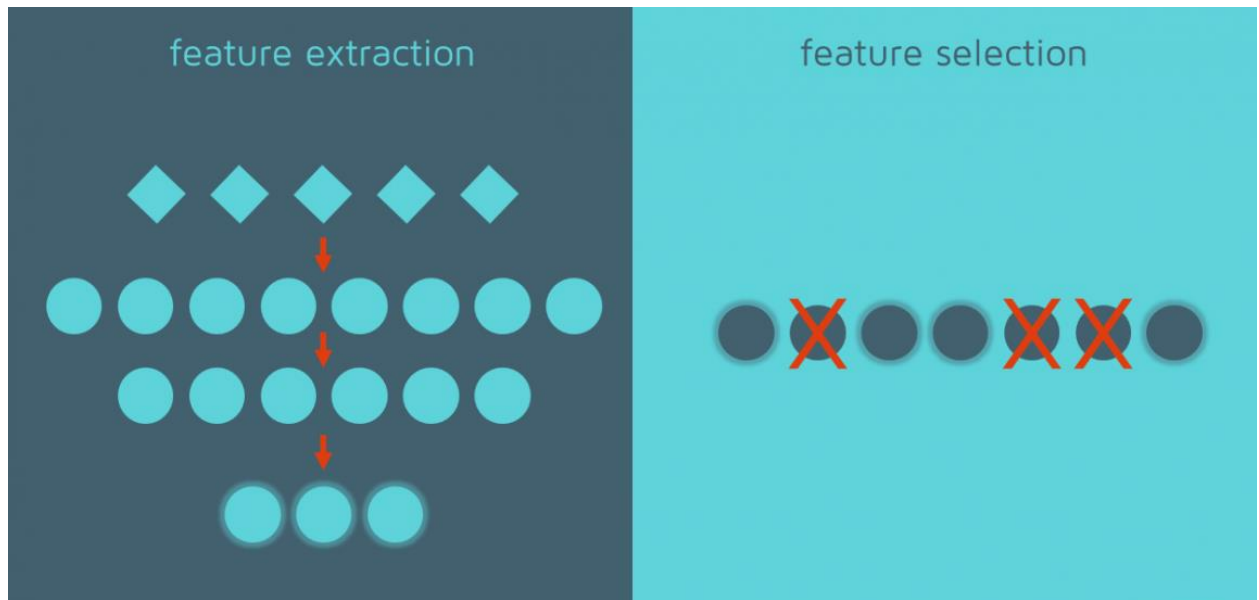


**Figure 3.4:** Feature Extraction and Selection [40]

### 3.1.5.1 Glaucoma detection through Textural Features/Statistical Features

Glaucoma can be diagnosed using a number of different measures, including the thicknesses and characteristics of the RNFL, the ONH, the vertically integrated rim area (VIRA), the CDR, the disc to horizontal ratio, and the disc to vertical ratio. LDA is used as a classifier to determine whether or not an OCT image depicts glaucoma or a healthy eye. This classification process involves forward selection and backward elimination. In order to diagnose glaucoma, researchers are looking into the correlation between the thickness of the retinal nerve fibre layer and the visual field. In the preventive therapy diabetic retinopathy research grid, the inner and outer rings are used to quantify the thickness of the retinal nerve fibre layer (RNFL). The regression analysis and Pearson's

correlation were used to determine the relationship between the mean sensitivity, the means deficiency and loss variance, and the thickness of the retinal nerve fibres. Textural features were proposed by Septiarini et al. [47] as a method for the automated identification of RNFL. In the outer area of the optic nerve head, a co-occurrence matrix has been obtained, and the question of whether to remove blood vessels is being explored. The Backpropagation Network (BPNN) classification technique is the most accurate method for detecting RNFL [47]. The investigation employed 40 retinal fundus images, and the sensitivity, specificity, and validity of the results were evaluated.

Kirar B. et al. [48] proposed a CAD technique for glaucoma based on EWT and DWT using fundus pictures. To choose the optimal features, SVD (Singular Value Decomposition) is applied to the selected features, followed by SVM classification [48]. Numerous performance evaluation metrics such as accuracy, sensitivity, specificity, Negative predictive rate (NPR), Rate of Negative Predictions (RNP), Matthews Correlation Coefficient (MCC), etc. are applied to 505 images from the MIAG image database [48]. Nirmala, K. et al. [49] introduced the wavelet-based contour let transformation (WBCT) approach for glaucoma identification. Adaptive gamma correction with weighted distribution has been used to improve image contrast. Utilizing a Gabor filter, the OD is split and blood vessels are eliminated. Experiments were conducted on the FAU dataset, and for evaluation purposes, accuracy, specificity, sensitivity, and positive predictive ratio were analyzed; however, only accuracy was compared to other approaches.

Classification of glaucoma based on PCA is explained using OCT images. Initially, median filtering and Otsu thresholding are used for preprocessing, while the required region is extracted from OCT images. The ROI-selected images are then subjected to PCA, and the resultant features are used for classifier training. The SVM classifier is utilised in order to determine if an image is normal or glaucomatous. The retrieved mean and energy characteristics are then supplied into the KNN classifier for picture classification.

Glaucoma patients are characterised by autonomic dysfunction, which has been related to the progression of the disease. Using dynamic pupillometry, Park analysed patients' responses of their pupils to a light flash in order to evaluate the status of the autonomous nervous system in glaucoma patients. A total of 97 glaucoma patients took part in the study, each contributing 21 eyes from their own unique glaucoma patient experience with cardiac autonomic dysfunction. Following a dark adaption period of two minutes, pupil responses to a brief flash of white light were observed and measured using dynamic pupillometry. In order to do statistical analysis, the SPSS application was utilised. The t-test was used to analyse the differences between the groups. When it was necessary to compare frequency distributions, the Chi-Squared testing was conducted out. It was determined, with the help of linear regression analysis, how much of an impact the various circumstances had on the pupil's parameters. A significance level of 0.05 for the P value was considered to be statistically significant. SPSS was utilised in order to carry out the statistical analysis.

### **3.2 Importance of Early Glaucoma Detection**

The importance of early detection of chronic uncomplicated glaucoma originates from the likelihood of favorable therapy outcomes in early patients. In contrast, late cases typically involve irreversible visual impairment. Due to the asymptomatic nature of chronic uncomplicated glaucoma, frequent screening tests are necessary. Appropriately referred to as "the thief in the night," glaucoma insidiously erodes the vision field and sharpness, with the afflicted detecting this loss irreversibly late. Many clinicians are under the false impression that glaucoma is a minor, rather uncommon, acute condition that is easily identified by the painful, red, and rigid eye. These are the hallmarks of glaucoma in its acute form. It is widely recognized that disease severity influences the diagnostic performance of OCT parameters in glaucoma which is often expressed by the Area Under the Receiver Operating Characteristic Curve (AUROC). Therefore, efforts have been made to examine the diagnostic accuracy of macular OCT measures and compare their performance with that of ONH and cpRNFL thickness at earlier (preperimetric and moderate perimetric) phases of glaucoma. Their findings demonstrate

that the diagnostic performance of macular and cpRNFL measures in early glaucoma is excellent and comparable [50].

**Table 3-2:** Glaucoma Detection Methodologies Summary 2

<b>Study by</b>	<b>Methodology</b>	<b>Dataset</b>	<b>Result</b>
Pal, A. et al. [51]	Mathematical morphology for OD Segmentation RIM-ONE	Database of 290 fundus images	Accuracy of 98%
Tjandrasa et al.[52]	Hough transform	30 Fundus Images	Accuracy of 75.56%
Raja, H. et al. [53]	Complex wavelet features and trispectrum	RIM-ONE	Accuracy 81%
X Chen at el. [54]	Glaucoma Based Deep Learning C-CNN	SCES and ORIGA	Accuracy of 89%
Hagiwara et al. [55]	Segmentation of OD, fovea and retinal vasculature using a 7-layer CNN	DRIVE	Accuracy of 92.68%

The vast majority of glaucoma diagnostic algorithms make use of a variety of distinct metrics, which may be deduced from the aforementioned review of disease diagnosis using OCT photographs. Calculations of this kind place a significant emphasis on the segmentation of the optic cup, optic disc, RC boundary, RV border, and RNFL. If they are not properly segmented, then they will be given the wrong classification. In order to avoid this, an approach for the classification of OCT images within an automated glaucoma diagnostic system has been presented. From a comprehensive literature study of glaucoma, it can be established that early identification is the only determining factor in glaucoma diagnosis. In this technique, the provided system is comprised of various sections that contribute to an increase in early glaucoma diagnosis efficiency.

Macular OCT can detect early glaucomatous damage that may not be visible on OCT scans of the disc region. In the presented approach, OCT pictures of the macula are used to determine the layers and thickness of the retina. The statistical analysis of OCT and Fundus pictures is accomplished in two distinct ways. SPSS programme is used to select relevant features. The discovered relevant characteristics are then supplied to the various classifiers. The results indicate that SVM is the most effective method compared to the alternatives. Comparing the results of various blocks, the classifier distinguishes between glaucomatous and healthy eyes. The data passes through various stages that make the system robust, more efficient, and contribute to the reduction of artefacts.

# CHAPTER 4: METHODOLOGY

The purpose of this work is to build a trustworthy statistical method for glaucoma diagnosis based on the concepts and procedures recommended by seasoned medical diagnosticians. The system was developed with the participation and approval of the local ophthalmology teams of three distinct institutions, with the primary objective of providing a decision tree and support platform for medical practitioners to identify glaucoma. Figure 4.1 depicts the block diagram of the proposed methodology. It consists of four main blocks and several sub-blocks, with each sub-block including a crucial procedure for producing the desired output.

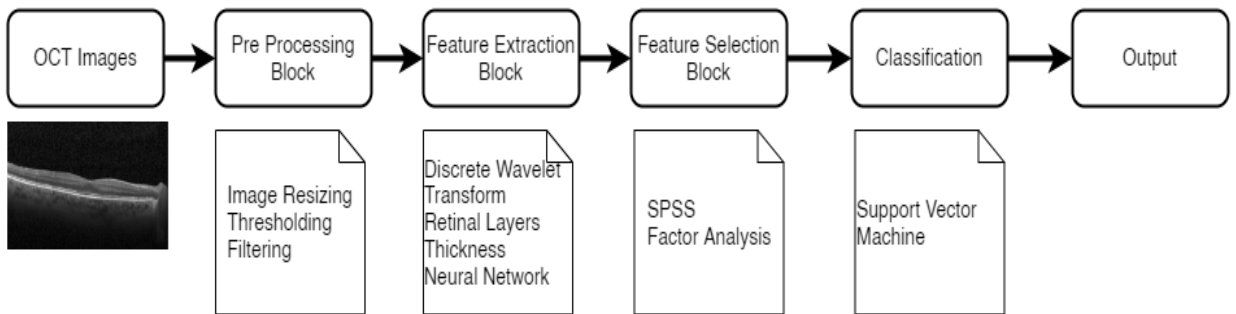


**Figure 4.1:** Block Diagram of Methodology

In order to develop a dependable system for early glaucoma diagnosis, the Main blocks are subdivided into several sub blocks. The created system consists primarily of two blocks, each of which contributes to the diagnosing procedure. In the first block, statistical analysis is used to extract various features based on structural and textural characteristics. As glaucoma is a degenerative illness, structural modifications precede functional modifications. Consequently, the early diagnosis of glaucoma depends on the detection of these structural abnormalities. Macular thickness is the most essential factor for early glaucoma diagnosis, according to the literature. Consequently, the thickness of



the macula is used as a statistical feature alongside the other features recovered using the wavelet transform. This section's block diagram is as follows:

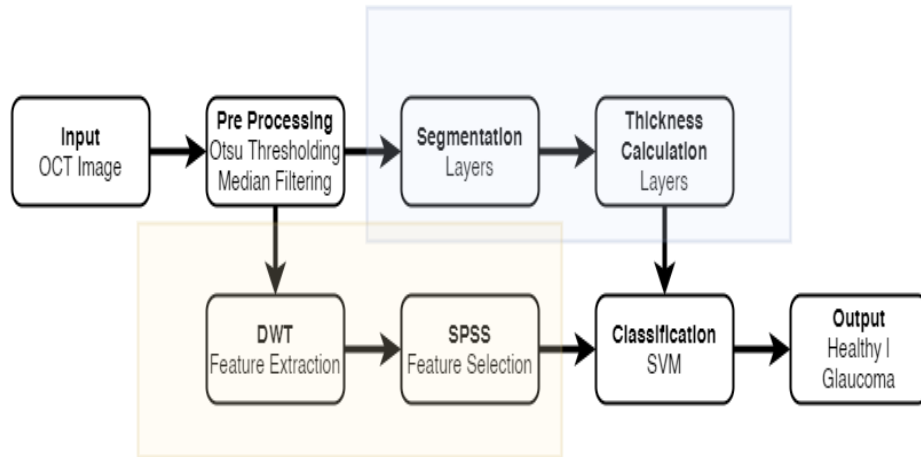


**Figure 4.2:** Block Diagram of Statistical Analysis

In the second block of statistical analysis, both fundus and OCT pictures are used for training and feature extraction using a DarkNet-53 convolution network. The model contributes to the system's robustness and time and cost savings. The model represents the result of numerous ideas developed over time by numerous researchers. The following is a block diagram depiction of the section.

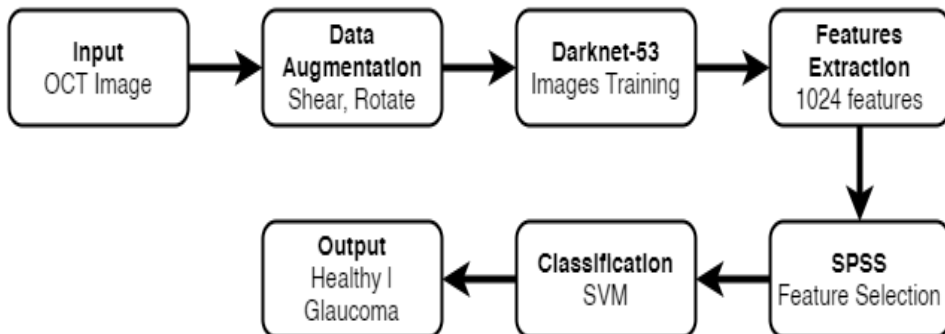


**Figure 4.3:** Block Diagram of DarkNet-53

On the basis of classifiers, the purpose of this study is to employ numerous blocks for recognizing structural and functional aspects, which leads to more accurate and

trustworthy findings for early glaucoma diagnosis. The description of methodological blocks is available in the subsequent subsections:

#### **4.1 Pre-Processing Block**

In this study, segmentation is performed based on similar grey levels, which is incredibly useful for recognizing features and detecting changes across many regions. Otsu thresholding is the algorithm applied to OCT images to distinguish between background and foreground pixels. It is the most common and fundamental segmentation method. It converts the grayscale image to the binary image format. It functions well in photographs containing few identifiable objects, such as OCT pictures. In Otsu thresholding, the mean and standard deviation of the input image as well as the threshold for segmenting the image are calculated. The threshold is given by:

$$T = Mean + 3(Standard\ Deviation) \quad (i)$$

Where T represents a threshold. The Otsu thresholding approach makes image quality irrelevant to segmentation. Now, thresholding divides a picture into two sets of pixels that are represented by a bimodal histogram (fore- ground and background pixels). Histogram is described as a graph comparing the number of pixels in the ROI image to the number of grey levels. The horizontal axis of the histogram displays the tonal variation, while the vertical axis displays the total number of pixels. For subsequent processing, the retinal region is automatically extracted from the separated foreground region.

In addition, the input image resolution must be comparable for the proposed glaucoma diagnosis model. As a result, a median filter with a window size of 5x5 is applied to the image in order to remove unwanted binary objects. Indeed, the primary benefit of the preprocessing block is enhancing the OCT pictures for the segmentation and localization blocks that follows:

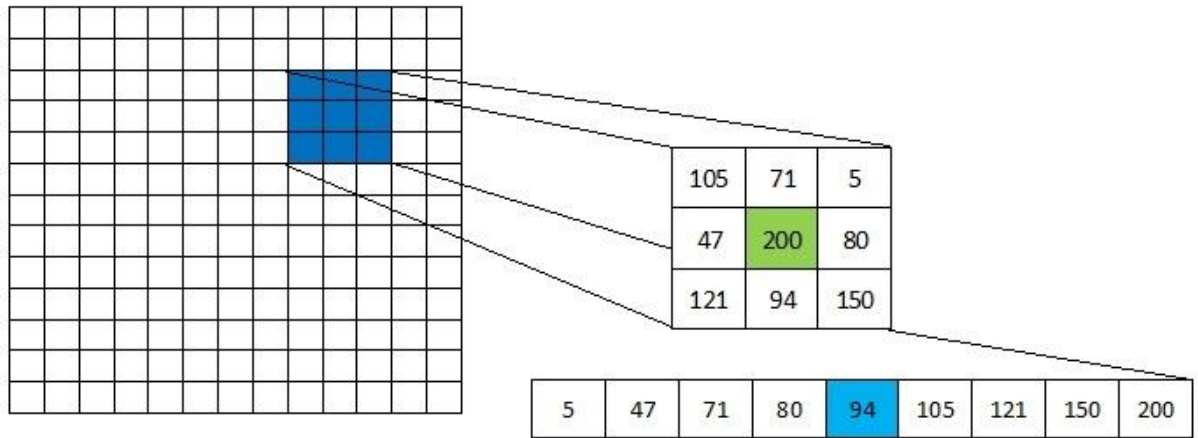


**Figure 4.4:** Median Filter Working – Edge Preserving and Noise Removal Filter [56]

#### 4.1.1 Proceedings of Pre-Processing Block

The pre-processing of the image is indeed the first and foremost block of most of the algorithms. The images need to be processed to minimize the computational power of the system. The steps involved in this methodology are explained in steps below:

1. Initially, all the images of the dataset are placed in a folder with the 70% training and 30% testing data. However, to extract all the mentioned features as discussed earlier the images are also placed in one folder with classes, glaucoma and healthy.
2. Beginning with the preprocessing, MATLAB functions for the required action are selected and performed on the images.
3. The image first gone through the process of resizing and then the thresholding is performed on the target image. Otsu thresholding is selected in the methodology as explained in the earlier section.
4. Meanwhile, the result images are stored and shown in the MATLAB images viewer.
5. To reduce noise and preserve edges, the median filter is employed after thresholding the image, a non-linear digital filtering approach.



The method relies on the user picking a Region of Interest (ROI) after photos have been preprocessed. Based on graph theory, the technology automatically segments the retinal layers. Using a graphical user interface, manually or semi-automatically adjust the segmented retinal layers, as seen in Fig. To determine the thickness value, the location of segmented boundaries is utilised. (Imp). The average thickness value of healthy and glaucomatous eyes is then employed for categorization purposes as a statistical characteristic.

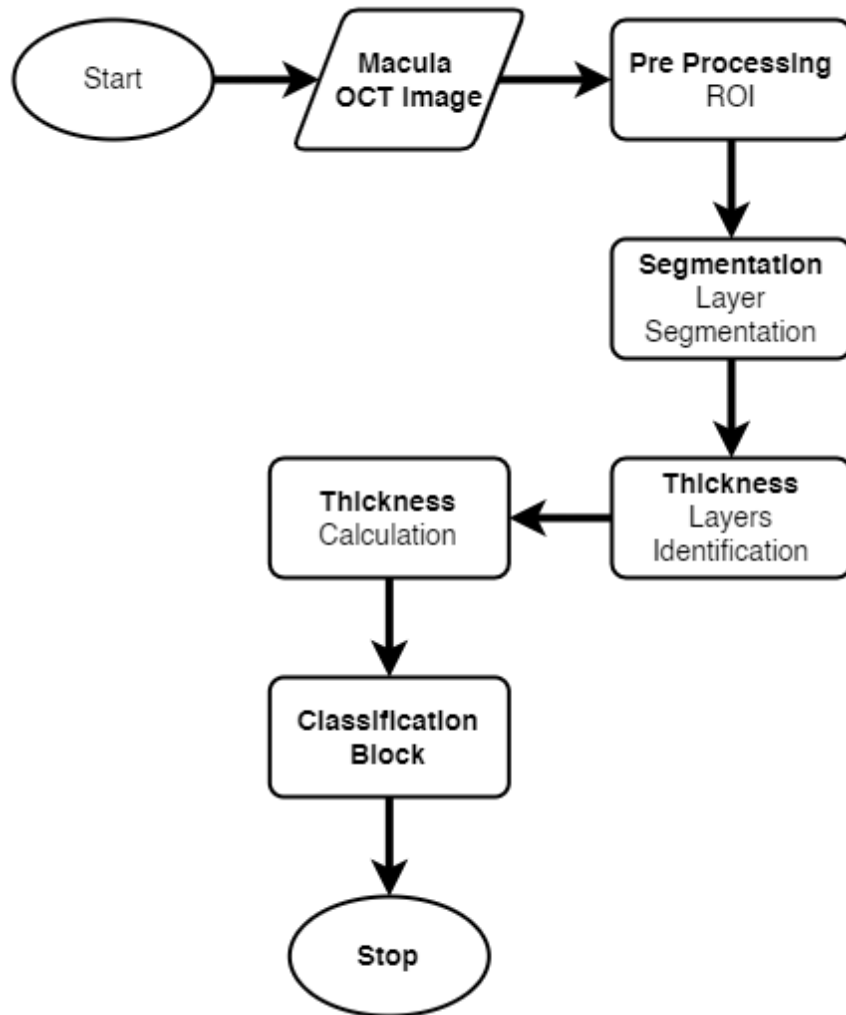


**Figure 4.6:** Flow Chart of Segmentation Block

#### 4.2.1 Proceedings of Segmentation Block

The segmentation of the retinal images is one the major contribution of the system where the macula size is calculated through the MATLAB functions prepared for the identification of mean and standard deviation of the retinal layers path. The steps involved in the processing of this block are:

1. The image in the initial step is resized and one of its channels is selected for the processing.
2. The type of the image is set to double in order to make the calculations right.
3. The whole image is then segmented into x and y range, that are passed in the function to extract the retinal layers of the images.
4. Then the image is smoothed in the function and filters are applied on it of [ 5 5 1] and [20 20 2].
5. After smoothening of images, the constants are selected and tagged with each retinal layer that are used for the defining of the region for the segmentation.
6. After this initial setting of constants, the smoothed image is then passed through the gaussian filter for denoising of the image.
7. The output of the more smoothed image is then passed through another gaussian filter and then created the adjacency matrices.
8. These matrices are passed to another function to get the hyper reflective layers and the output is saved as the rPath.
9. These paths are identified for each layer and stored as a constant to define the region. The code then finds the shortest path to get the layers identification.
10. The identified layers are then saved in a .mat file. That is passed to the next function where the retinal thickness is calculated.
11. In this function the calculated layer paths are concatenated and format the paths for the analysis and quantify the retinal layers thickness.
12. Once the retinal layers thickness is quantified the result is stored in MATLAB file as an excel that is used as an input in another block as feature.

### 4.3 Feature Extraction Block

The fundamental objective of feature is to extract the most relevant information from the source data and represent it in a space with lower dimensionality. This may be accomplished by reducing the number of dimensions in the space. When an algorithm's input data is too large to be processed because it contains what is thought to be redundant information (a lot of data but not much information), the input information is translated into a set of features is called, also known as a feature extraction. This allows the input data to be processed by the algorithm. Extraction of features refers to the process of converting incoming data into a collection of distinct characteristics. It draws forth the relevant information that differentiates each category.

Once pre-processing and the necessary amount of segmentation have been accomplished, a feature extraction technique is used to the segments to obtain features, followed by the application of classification and post-processing techniques. Focus must be placed on the phase of feature extraction because it has an observable effect on the system's performance. In addition, the generated discriminant features affect the accuracy of the classification system and play a significant role in identifying and separating glaucoma pattern features from non-glaucoma pattern features. In the created system, features are extracted utilizing three distinct techniques, Discrete Wavelet Transform, Macular Thickness, and the DarkNet-53 model.

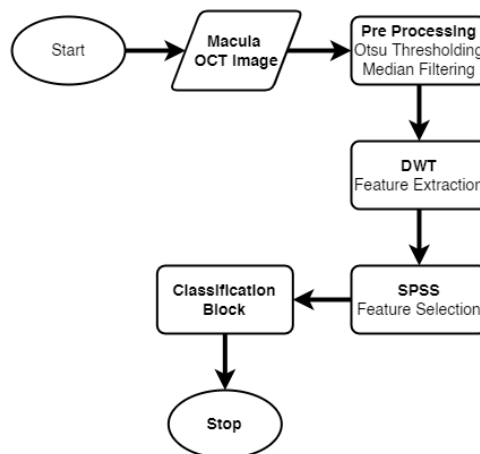


**Figure 4.7:** Flow Chart of Feature Extraction Block

## 4.4 Discrete Wavelet Extraction

DWT is capable of extracting both frequency and position information. Rather than global picture properties, it collects details in horizontal, vertical, and diagonal orientations. The fundamental objective of using DWT as a textural element in the proposed method is to capture variations in OD that can be utilised to differentiate between normal and glaucoma cases. In a digital image, low-frequency variations are smooth color changes, and high-frequency variations are abrupt color changes. DWT is a technique for isolating fine features and smooth variations in an image. This linear transformation operates on data vectors with lengths that are integer powers of two. It splits each piece of data into discrete frequency modules and then analyses each one with scale-appropriate resolutions. The DWT was computed using a cascade of filtering followed by subsampling by factor 2.

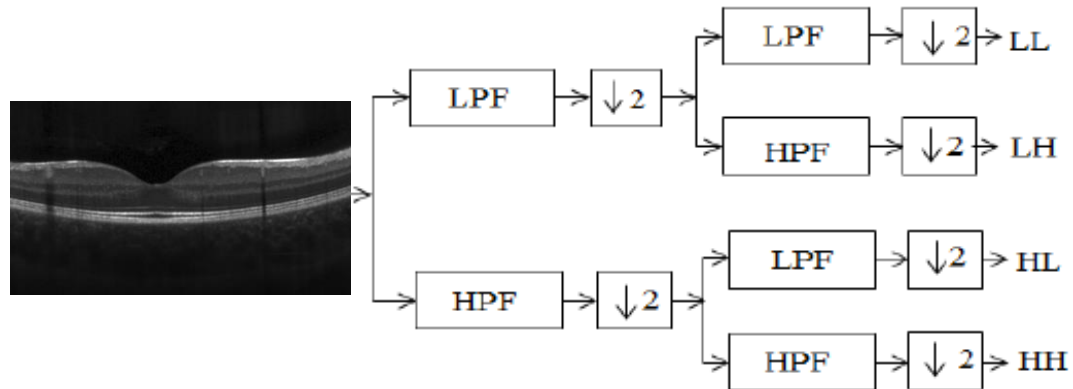


**Figure 4.8:** Architecture of DWT and the Filters Level

In sub band decomposition, the signal is represented by the DWT. Using a wavelet packet to generate the DWT makes sub-band analysis possible without requiring dynamic decomposition. The discrete wavelet packet transformations (DWPT) implement a frequency axis decomposition that is adaptive. The specific decomposition will be selected according to an optimization criterion. The Discrete Wavelet Transform (DWT) is a time-scale representation-based technique for multi-resolution sub-band decomposition. It has evolved into a robust signal processing tool with numerous applications in domains including audio compression, pattern recognition, texture



discrimination, and computer graphics, among others. In image/video coding applications, the 2-D DWT and its cousin, the 2-D Inverse DWT (IDWT), are particularly essential. This image processing reduces the size and quality of image data, allowing it to be stored in a little amount of memory. In this stage, the image is compressed and decompressed, with the results being displayed at the output.

In this experiment, wavelets are utilised to extract information from OCT images in the frequency domain. The pre-processed OCT images are subjected to DWT decomposition, and the resulting wavelet coefficients are then used to extract wavelet domain features. The input image is subjected to 2D-DWT since images are 2-dimensional (2D) data. To obtain 2D-DWT, 1D-DWT is applied row-by-row, followed by column-by-column. A pair of low pass and high pass filters are utilised for DWT decomposition. The recommended system leverages the Haar wavelet for decomposition. The coefficients of the low pass and high pass Haar wavelet filters utilised in this study are provided in Table 1. No matter the level of decomposition, the dimensions of a DWT-transformed image are identical to the dimensions of the original image. As a result, the processed wavelet image has a resolution of 64 by 128, suggesting that 8192 wavelet coefficients are available as features. Due to the enormous dimensionality of the data, classification precision and calculation time would necessarily drop. To avoid these circumstances, prominent or identifying characteristics are chosen.

## **4.5 Statistical Features Extraction**

Digital image processing and analysis of information in images are techniques that are gaining importance in an expanding number of technical and scientific domains, including nearly all of the biological sciences. At this time, we compute the statistical characteristics that are commonly employed in both conventional and GLCM. Standard qualities include the average intensity (also known as the mean), standard deviation, smoothness, third moment, homogeneity, and entropy. GLCM features can be used to quantify the damage caused by the degeneration of fibre neurons in the optic disc of a glaucomatous eye. GLCM provides data on the relative positioning of neighboring pixels in an image.  $P(I, j)$  is the GLCM for images of size  $m \times n$ . The proposed system extracts and exploits the five GLCM features shown below [29]. The GLCM features that are

retrieved and included into the model are listed below. Table 4.1 contains the calculated formulas for the specified characteristics.

**Table 4-1:** Standard and GLCM Features

Standard Features	Formula	GLCM Features	Formula
Mean	$m = \sum_{i=0}^{L-1} x_i \rho(x_i)$	Homogeneity	$H = \sum_{1,j=0}^{N-1} \left( \frac{P_{i,j}}{1} + (i - j)^2 \right)$
Standard Deviation	$\sigma = \sqrt{\sigma^2}$	Contrast	$C = \sum_{1,j=0}^{N-1} P_{i,j} (i - j)^2$
Smoothness	$R = 1 - \frac{1}{(1 + \sigma^2)}$	Dissimilarity	$H = \sum_{1,j=0}^{N-1} P_{i,j}  i - j $
3 <sup>rd</sup> Moment	$\mu = \sum_{i=0}^{L-1} (x_i - m)^3 \rho(x_i)$		
Uniformity	$U = \sum_{i=0}^{L-1} \rho^2(x_i)$		
Entropy	$e = \sum_{i=0}^{L-1} \rho(x_i) \log_2 \rho(x_i)$		

## 4.6 Feature Extraction Using DarkNet-53 Model

Utilizing a deep learning (DL) neural network as a classification block is the most cutting-edge method for carrying out statistical analysis. The majority of the time, it appears that the outcomes of DL techniques have good accuracy and performance. DL has pushed the boundaries of what is possible in the fields of image processing and method automation, and it has produced extraordinary achievements. Artificial neural networks, which have a structure similar to that of the brain and operate in the same manner as the brain does, provide the backbone of DL. Because trained neural networks are employed instead of programmed systems, the results they produce are more accurate than those obtained using more conventional methods. The data set is composed of two distinct sets: the training set and the testing set. Following the implementation of the augmentation strategies, the model is trained. Validating the model based on the training

photos uses ten percent of the images that are collected during the training phase. After that, we assessed it using several test photographs.

#### 4.6.1 Structure of DarkNet-53 Model

Layer	Filters size	Repeat	Output size
Image			$416 \times 416$
Conv	$32 \ 3 \times 3/1$	1	$416 \times 416$
Conv	$64 \ 3 \times 3/2$	1	$208 \times 208$
Conv	$32 \ 1 \times 1/1$	[Conv Conv] $\times 1$	$208 \times 208$
Conv	$64 \ 3 \times 3/1$		$208 \times 208$
Residual		[Residual]	$208 \times 208$
Conv	$128 \ 3 \times 3/2$	1	$104 \times 104$
Conv	$64 \ 1 \times 1/1$	[Conv Conv] $\times 2$	$104 \times 104$
Conv	$128 \ 3 \times 3/1$		$104 \times 104$
Residual		[Residual]	$104 \times 104$
Conv	$256 \ 3 \times 3/2$	1	$52 \times 52$
Conv	$128 \ 1 \times 1/1$	[Conv Conv] $\times 8$	$52 \times 52$
Conv	$256 \ 3 \times 3/1$		$52 \times 52$
Residual		[Residual]	$52 \times 52$
Conv	$512 \ 3 \times 3/2$	1	$26 \times 26$
Conv	$256 \ 1 \times 1/1$	[Conv Conv] $\times 8$	$26 \times 26$
Conv	$512 \ 3 \times 3/1$		$26 \times 26$
Residual		[Residual]	$26 \times 26$
Conv	$1024 \ 3 \times 3/2$	1	$13 \times 13$
Conv	$512 \ 1 \times 1/1$	[Conv Conv] $\times 4$	$13 \times 13$
Conv	$1024 \ 3 \times 3/1$		$13 \times 13$
Residual		[Residual]	$13 \times 13$

Conv

Con2d  
Layer

BN  
Layer

LeakyReLU  
Layer

Residual

Conv  
(1 × 1)

Conv  
(3 × 3)

Add

**Figure 4.9:** Structure of DarkNet-53 [57]

#### 4.6.2 Data Augmentation

A procedure known as data augmentation is one that helps to enhance the variety of data that is used for training a model without the need to collect fresh data. It works as a kind of stabilizer. The effectiveness of the model is improved as a result. It is helpful in avoiding the problem of over-fitting. A neural network processes enhanced images as if they were separate images. The enhanced Image data store is utilised for the purpose of doing data augmentation for this designed system. Images should be resized so that they are suitable with the input size of the deep learning network you are using. When an image is shifted, all of its pixels are moved in the same general direction. There are two different kinds of shifts possible: width shift and height shift. Changing the position of an object is made easier when shifting its position. When we flipped an image, we reversed

either the columns or rows of pixels, depending on whether the image is being flipped horizontally or vertically. It is analogous to spinning an object either clockwise or counterclockwise around its axis. The process of rotating an image involves turning it either clockwise or counterclockwise within a range of 0 to 360 degrees. In zooming technique, images are either zooms in or zooms out. A value that is more than 1 will zoom out an image, while a value that is equal to 1 will have no impact. A value that is less than 1 will zoom an image in. Add randomized pre-processing procedures to the training image data in order to help prevent the network from overfitting to the training images and from learning the exact details of the training images.

### **4.6.3 DarkNet-53**

In order to further enhance the effectiveness of the glaucoma diagnosis process, data augmentation procedures are implemented. A convolutional neural network with 53 layers of depth is denoted by the name DarkNet-53. The Darknet-53 model is trained using an enhanced version of the training dataset. The model contains a total of 53 layers, including the following: 1 input layer, 94 Cov2d layer, 94 batch normalization layer, 94 activation layer, 11 mixed layer, 8 average pooling layer, 4 max pooling layers, 2 concatenate layer, 3 global average pooling layer, and 1 dense layer. The dark-net architecture is utilised in the extraction of the features. After putting them through their paces across all of the intended models, the test OCT pictures are then used to do the evaluation of the model. Finally, the trained model is able to detect fundus images regardless of whether they are normal or glaucomatous; nevertheless, the number of extracted features is more than before, which will have an impact on the classification accuracy. As a direct consequence of this, a dimension reduction analysis using the SPSS software is carried out on the collected features in order to identify key features.

## **4.7 Feature Selection**

The primary objective of features selection is to pick a subset of input variables by omitting features with insufficient or no predictive information, while preserving or improving classification accuracy. John et al. categorized feature significance as either strong or weak. Strong relevance indicates that a feature cannot be eliminated from the

set of features without compromising classification accuracy. Weak relevance indicates that a characteristic can occasionally help to classification accuracy [58]. A good feature set comprises information that allows one object to be distinguished from others. The chosen set of features should consist of a small number of features whose values easily differentiate between patterns of various classes, but are identical for patterns within the same class.

In recent years, the usage of feature selection algorithms in medical datasets has increased. The challenging aspect of feature selection is identifying the appropriate subset of relevant and non-redundant information that will produce an optimal solution without increasing the complexity of the modelling work. Therefore, practitioners must be aware of feature selection strategies that have been successfully applied to medical data sets, as well as future developments in this field. Findings indicate that the majority of existing feature selection strategies focus on univariate ranking, which disregards relationships between variables, disregard the stability of selection algorithms, and require a larger number of features to attain high accuracy. Nevertheless, the development of a universal technique that achieves the best classification accuracy with the fewest features remains an ongoing process.

Feature selection is the process of selecting the subset of a given number of features that leads to the highest possible generalization or, in other words, the lowest risk. The Fisher procedure, which computes a score for a feature as the ratio of interclass separation and interclass variance, where features are evaluated independently and the final feature selection is determined by averaging the highest-ranked features, is an efficient and quick filtering method. In unsupervised learning circumstances, when there are no class labels to guide the search for relevant information, picking features is a substantially more difficult problem.

#### **4.8 Correlation based Feature Selection Using SPSS**

Not all of the previously recovered features are essential for attaining the best classification result in the subsequent phase. Consequently, feature selection is achieved by lowering the dimension of the features. In this work, the correlation matrix-based

dimension reduction factor analysis method is applied. This technique was selected since it has been utilised in several investigations, particularly in the medical profession. Dimensionality reduction can be employed for noise reduction, data visualization, cluster analysis, or as a stepping stone to facilitate additional investigations. Factor analysis is a heuristic method for determining the use of individual features to forecast class based on the intercorrelation between features. The removal of features that are interconnected yet unimportant.

The correlation-based feature selection method assesses feature subsets by selecting feature subsets with attributes that are significantly correlated with the classification but not with one another. The data is also exposed to a number of SPSS tests, such as the T test and the ANOVA, in order to find the most pertinent characteristics and improve classification precision.

By Kaiser's criteria, SPSS identifies eigenvalues greater than 1 as the relevant characteristics in this inquiry. Now, the eigenvectors corresponding to the biggest eigenvalues (the principal components) can be utilised to reconstruct a significant portion of the original data's variance. The selected collection of critical features is utilised to distinguish between glaucoma and non-glaucoma OCT images. A few of the benefits are enhanced classifier learning, enhanced predicted accuracy, a faster execution time, and reduced computer costs. For training OCT images, feature extraction and feature selection are performed, and the corresponding features are saved for classifier training and testing.

## **4.9 Classification Block**

The final step of the glaucoma diagnosis paradigm is classification, which entails determining whether the testing image belongs to the normal or glaucoma category. A linear or nonlinear model will be used to identify the disease using the classifier. The accuracy of a system's classification depends not only on the selection of a feature set, but also on the selection of an appropriate classifier. To achieve the best outcomes, we analyzed these attributes using a number of classifiers.

Various classification algorithms, such as Support Vector Machine (SVM), K-means Clustering (KNN), and Bayesian classifier, have been tested and utilised in earlier publications. Because it is simple, the k-NN method is frequently used for categorization. The k-NN technique requires multiple types of input data, including the number of neighbors  $k$ , a distance matrix, and a training dataset. If  $k = 1$ , the classification based on the nearest neighbor of the training data is utilised to determine the class of the test data.

Due to its greater generalization and rapid convergence in high-dimensional data, the SVM classifier is utilised in the system under development. SVM is renowned for its superior handling of multidimensional data, binary classification, and durability, which is achieved by employing multiple kernels. SVM produces a binary decision on glaucoma based on the input feature vector. As information, the classifier employs prior characteristic elements. It can manage both continuous and categorical variables with ease. The features derived from the various system blocks, including macular thickness, wavelet features, GLCM features, and key SPSS characteristics, are then fed into SVM for training. During the training phase of SVM classification, the relationship between the given normal and glaucoma features is determined and optimized through hyperplane. SVM constructs the ideal hyperplane iteratively in order to minimize an error. It optimally divides the provided wavelet characteristics and others into two classes.

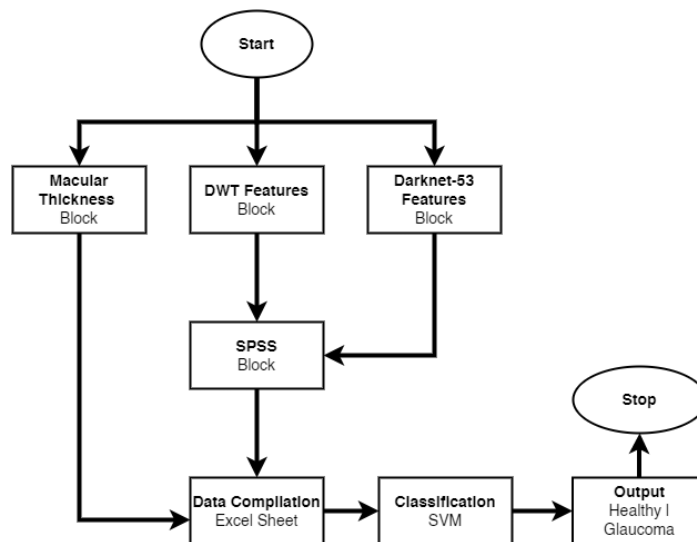


**Figure 4.10:** Classification Block Diagram

### 4.9.1 Proceedings of Classification Block

The following is a rundown of the process that we went through in order to classify data using the Classification Learner app:

1. Prior to opening the app, the first thing we did was import the data that was going to be used in the workspace.
2. Following that, we navigated to the Apps menu in MATLAB and selected the classification learner. Because we have installed the Statistics and Machine Learning toolbox, we now have access to it without having to do anything. We also have the option to launch the application by typing `classificationLearner` at the command prompt.
3. We choose the variable from the dataset that will be used in the learner application for the evaluation. While the dataset attributes are being chosen, the response and predictors are being identified on an ongoing basis automatically. The responses that are shown here represent the parameters that were used to classify the data.
4. The validation % is determined according to the requirement for the cross-validation type, which is for datasets that are larger. To ensure that the trained model does not become overfit, the validation phase involves performing a check on the model before the testing phase.
5. Once the dataset and validation method had been selected, a scatter plot of the training data characteristics appeared in the session. This plot can be altered to suit the user's needs by navigating to the appropriate section of the navigation bar.
6. Because choosing a classifier was such a time-consuming operation, we chose all 24 of the classifiers that were accessible within the application and then began the process of training the models. A parallel pooling session was started in MATLAB so that we could get started with the training.
7. We were able to view the training accuracy results for all 24 models on the left-hand side of the programme. We saw that many classifiers had the highest



accuracy, but linear SVM had the best area under the curve (AUC), thus we decided to use linear SVM as our trained model.

8. Once we had chosen the classifier, we went through and looked at all of the available graphs.
9. Finally, we exported and saved the trained model so that it may be used for prediction. That can be put to use to make predictions based on the data that was provided.

In the proposed system, classification is performed independently on the dataset and extracted features, accuracy is evaluated using all of the classifiers supplied in the MALAB classification toolbox, and the SVM with the highest accuracy is selected as the classifier. The SVM classifier outperformed the other classifiers based on the dataset and characteristics utilised in our experiment. Due to its higher generalization and rapid convergence in high-dimensional data, the SVM classifier is utilised. In addition, the categorization is performed by extracting features from many platforms, which makes the established framework distinct, dependable, and useful for the early detection and progression of glaucoma disease by ophthalmologists.

# CHAPTER 5: RESULTS AND ANALYSIS

In this very important section, we discussed the performance of the proposed glaucoma diagnostic system based on DWT, Darknet-53, and SVM classifiers, as well as the detailed analysis of acquired results from all blocks after conducting multiple experiments in each block to compute the glaucoma and healthy eye identification and classification of the introduced framework. In this investigation, the following datasets were examined:

- Macular OCT Images by Kermany and Daniel – Germany

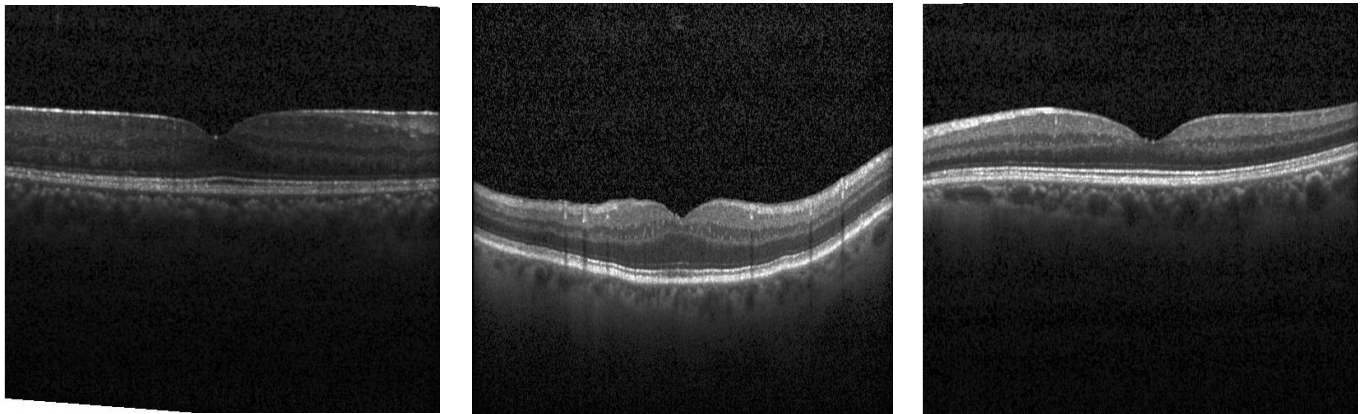


**Figure 5.1:** OCT Images [59]

As discussed, Macula OCT images are used for Layers segmentation and Macular thickness identification. The figure 5.1 shows the Macula OCT-image used for diagnosis process. The OCT images are preprocessed as described in the techniques section. To retrieve the focused region for layers' computation and extraction of wavelet GLCM features, we first extracted the focus region and then cropped the pictures to locate the

ROI. After the dataset has been cropped and shrunk, histogram equalization and pre-thresholding are used to determine the impact of noise on the image, which is reduced during the segmentation step.

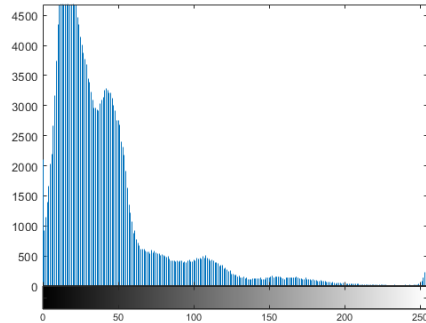


**Figure 5.2:** Image Histogram

The performance of the suggested system gets better when the fraction of critical features used for classification gets higher, and as the amount of DWT decomposition that's used gets higher as well. Because the DWT produces redundant data at higher and higher levels of decomposition, the performance of the algorithm is negatively impacted by larger degrees of degradation and by more than 50 percent of the top-ranked features. The filter bands of DWT can be seen in the figure 5.3.

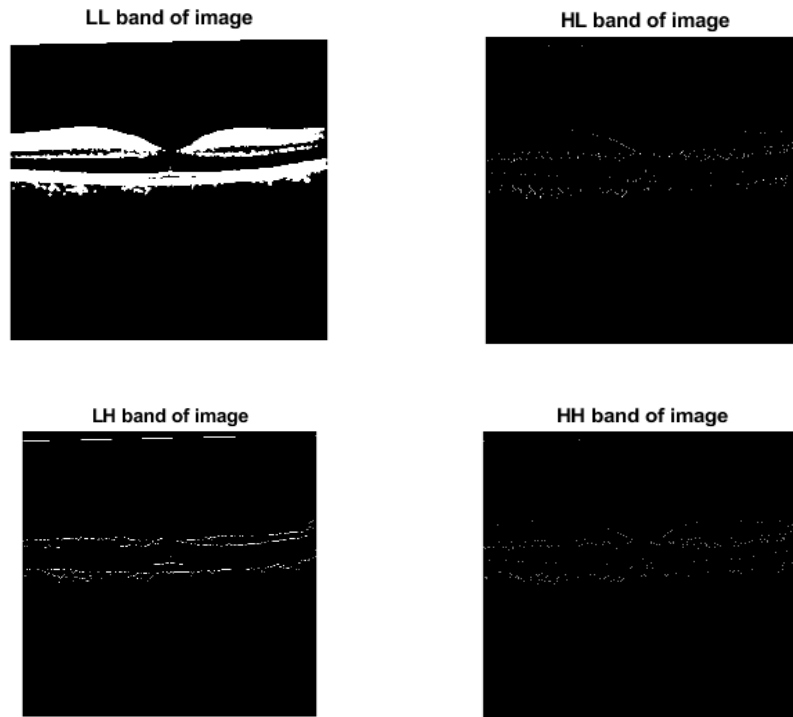


**Figure 5.3:** DWT Filter Bands

The ultimate goal of employing the DWT was to identify the distinguishing characteristics between glaucoma and a healthy eye. The statistical characteristics are extracted in two different ways. (i) Manually with the assistance of ophthalmologists for the detection of OCT layers, and (ii) automatically by estimating the ROI and macular thickness using predefined formulas for standard, GLCM, and a few statistical characteristics can be seen in the table 5.1.

**Table 5-1:** Mean and Standard Deviation of Statistical Features of Glaucomatous Eyes

Features	Mean	Standard Deviation
Contrast	0.172	0.013
Correlation	0.077	0.029
Energy	0.77	0.012
Homogeneity	0.94	0.003
Mean	0.002	0.0009
Standard deviation	0.08	0.0034
Entropy	3.51	0.07
RMS	0.08	6.1e <sup>-16</sup>
Variance	0.006	1.1e <sup>-5</sup>
Smoothness	0.927	0.056
Kurtosis	6.063	1.651
Skewness	0.449	0.149

The macular thickness is the most important statistical variable to measure, as determining the exact location of the inter-retinal boundaries is one of the most difficult aspects of OCT image processing. Our research is novel in that we combine macular thickness with statistical characteristics to develop a robust system. Using the same procedure, 78 manually and automatically marked images are compared. 280 features were extracted using DWT and then analyzed to determine the most useful feature set. The automatically marked macular images can be seen in figure 5.4.

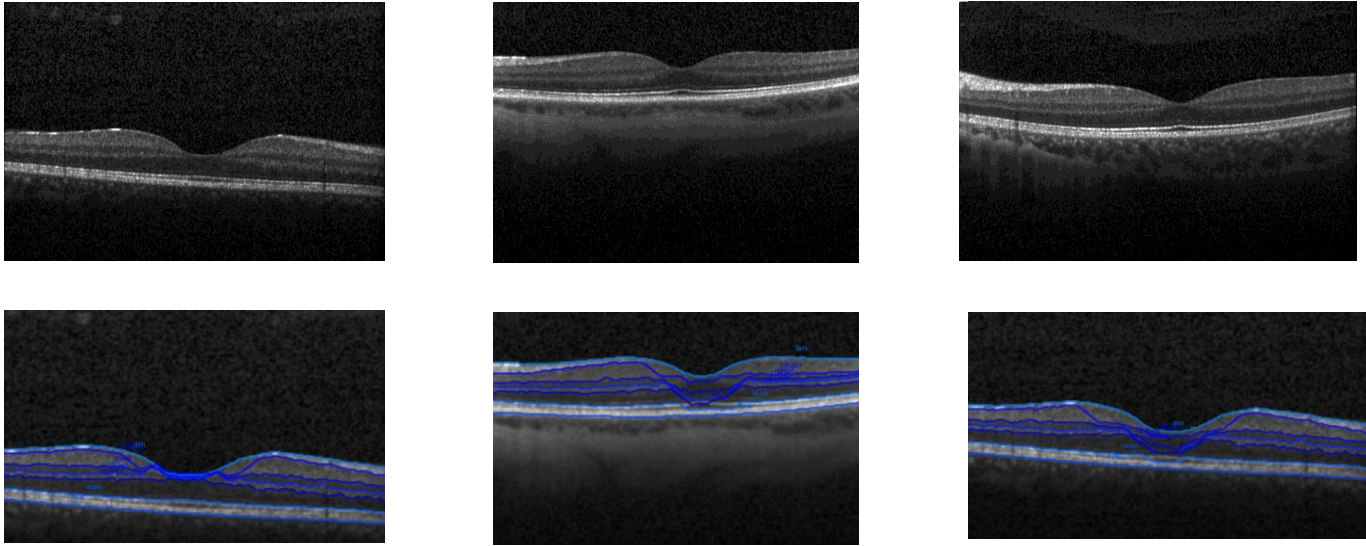


**Figure 5.4:** Automatically Marked Macular Layers

The mean and median of the healthy and glaucomatous eyes macular layers path can be seen in the tables below for observation. The overall mean for glaucoma eye is 12.60 and standard deviation is 6.90 whereas the overall mean and standard deviation for healthy eye is 17.28 and 5.71 respectively.

**Table 5-2:** Mean and Std. Deviation of the Retinal layers Path of Glaucomatous Eye

Layers	Mean	Standard Deviation
ilm – nflgcl	11.33	6.55
nflgcl – iplinl	13.03	10.09
iplinl – inlopl	6.38	4.04
inlopl – oplonl	7.85	4.43
oplonl – isos	19.73	8.28
isos - rpe	17.31	8.03

**Table 5-3:** Mean and Std. Deviation of the Retinal layers Path of Healthy Eye

Layers	Mean	Standard Deviation
ilm – nflgcl	12.03	4.03
nflgcl – iplinl	14.80	4.57
iplinl – inlopl	8.28	2.34
inlopl – oplonl	19.95	6.87
oplonl – isos	21.90	7.79
isos - rpe	26.77	8.67

The images are trained to obtain dense layer features using the DarkNet-53 framework and a predefined MATLAB classification module following the DWT and human feature selection. The images were trained with two folds, each with six epochs, 200 iterations per epoch, and a total of 1,200 iterations. With  $lr = 0.0001$ , the training period for the initial fold was around 10 minutes 30 seconds. The average training accuracy was 92.87 percent, while the classification accuracy was 91.2% utilizing an optimized SVM with feature dimensionality reduction and feature selection to boost classification accuracy. Factors in SPSS were used to minimize dimensionality, and T-Tests were performed to determine the frequency of closely related attributes and extracted features.

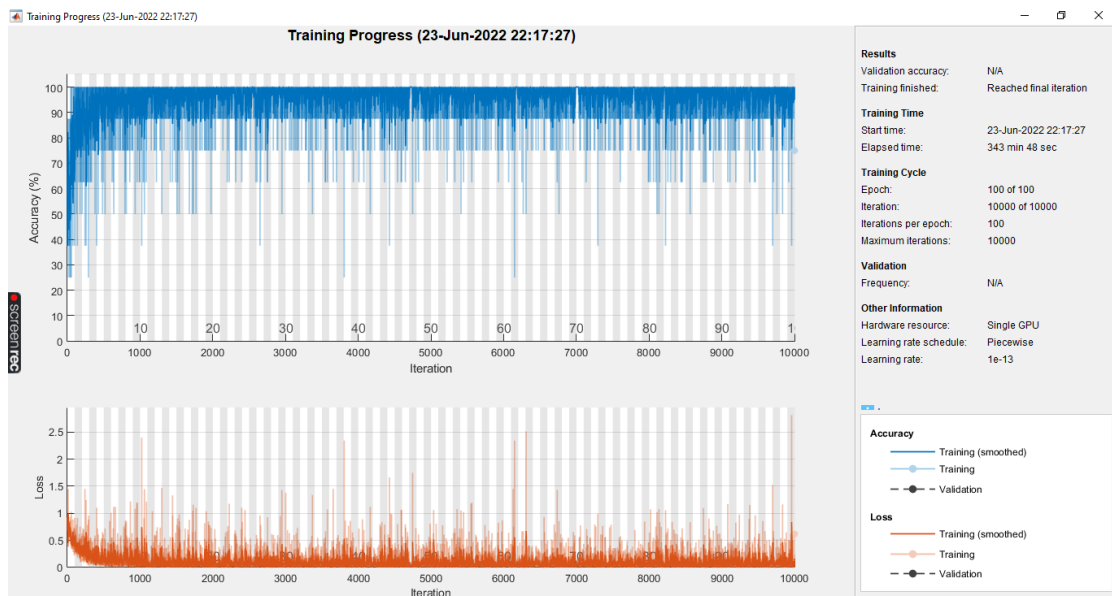


**Figure 5.5:** DarkNet-53 Training Fold 1

According to the preceding table, the residual value of the output's dependent variable is 0.025 and the expected value's standard deviation is 0.877. Before classification, the investigation was conducted on 1600 pictures that were rotated and enhanced. 782 out of 1024 features are eliminated, leaving crucial features available. The relevant characteristics are then incorporated into the classification in order to attain the best level of classification accuracy possible.

The features extracted using DarNet-53 and DWT are then passed to the very important step of the feature's reduction using dimensionality reduction in SPSS. Factor analysis examines which underlying factors are measured by a number of observed variables. Such "underlying factors" are often variables that are difficult to measure. As shown in figure 5.6 is the first output of the SPSS for the plugged-in data of DWT features, for DarkNet-53 the features are huge in number. Each component has a quality score called an Eigenvalue. Only components with high Eigenvalues are likely to represent real underlying factors.

**Total Variance Explained**

Component	Initial Eigenvalues			Extraction Sums of Squared Loadings			Rotation Sums of Squared Loadings		
	Total	% of Variance	Cumulative %	Total	% of Variance	Cumulative %	Total	% of Variance	Cumulative %
1	4.297	33.052	33.052	4.297	33.052	33.052	3.241	24.927	24.927
2	2.873	22.102	55.154	2.873	22.102	55.154	2.944	22.643	47.570
3	1.286	9.893	65.047	1.286	9.893	65.047	2.251	17.315	64.885
4	1.000	7.693	72.740	1.000	7.693	72.740	1.021	7.855	72.740
5	.998	7.679	80.419						
6	.886	6.816	87.236						
7	.621	4.773	92.009						
8	.550	4.233	96.242						
9	.229	1.763	98.005						
10	.133	1.022	99.027						
11	.085	.657	99.684						
12	.027	.207	99.892						
13	.014	.108	100.000						

Extraction Method: Principal Component Analysis.

**Figure 5.6:** Factor Analysis Output I: Total Variance

A common rule of thumb is to select components with Eigenvalues of at least 1. As shown in Figure 4.6, the SPSS factor analysis reveals that only four features have eigen values greater than 1, making them the most important for disease detection.

A scree plot represents the Eigenvalues (quality ratings) that we just observed. Again, figure 5.7 demonstrates that the Eigenvalues of the first four components are greater than 1. These are considered "strong considerations." Following the fifth component, Eigenvalues decline drastically. The significant decline between components 1 through 4 and components 5 through 16 clearly indicates that four elements explain our inquiries.

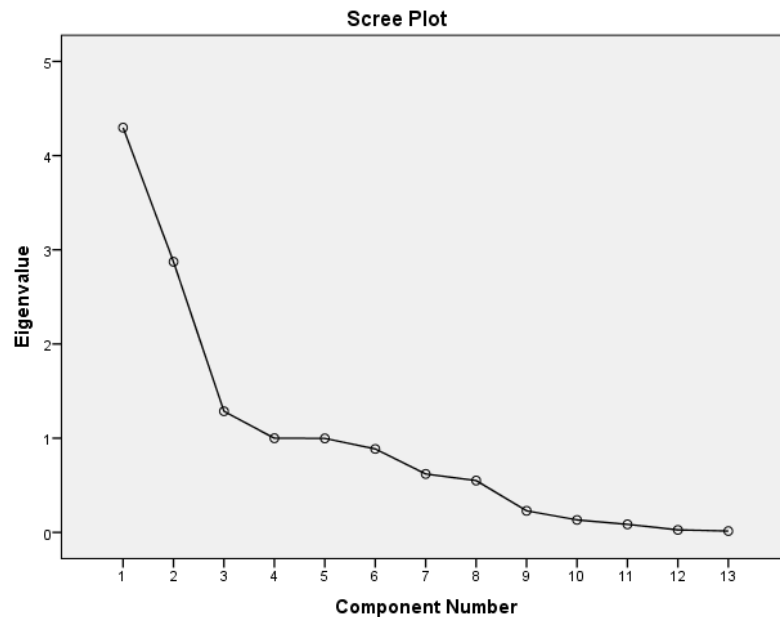


**Figure 5.7:** Factor Analysis Output II: Scree Plot

Image 5.8 depicts the Pearson correlations between the items and the components using the component matrix. Inexplicably, these correlations are referred to as factor loadings. Each input variable should ideally represent a single factor. Sadly, that is not the case in this instance. Energy measures (correlates with) components 1 and 3, for example. Even worse, homogeneity and entropy jointly measure components 1, 2, and 3. If a variable contains multiple significant factor loadings, we refer to these as cross loadings. This is problematic since it complicates comprehension. The answer to this problem is rotation, as depicted in image 5.9.



**Component Matrix<sup>a</sup>**

	Component			
	1	2	3	4
Energy	.890		.134	
Homogeneity	.882	-.194	.262	
Kurtosis	.743	.570		
Entropy	-.740	-.256	.305	
Variance	.681		.227	
Contrast	.149	.900	-.314	
Skewness	.501	.790	-.147	
Mean	-.554	.682	.402	
Standard_Deviation	.538	-.665	-.394	
Correlation	.527	-.122	.652	
Smoothness	-.126	.257	.440	
RMS				.990
IDM				-.138

Extraction Method: Principal Component Analysis.  
a. 4 components extracted.

**Figure 5.8:** Factor Analysis Output III: Component Matrix

Now, there are other rotation methods, but the most prevalent is the varimax rotation, which is an abbreviation for "variable maximization." It attempts to rearrange the factor loadings so that each variable measure precisely one factor - the optimal situation for comprehending our factors. And as we shall see, our varimax rotation works flawlessly with our data.

**Rotated Component Matrix<sup>a</sup>**

	Component			
	1	2	3	4
Homogeneity	.888	.156	-.265	
Correlation	.818		.196	
Energy	.800	.297	-.298	
Variance	.690	.155	-.155	
Skewness	.165	.918	.143	
Contrast	-.232	.905	.222	
Kurtosis	.473	.807		
Entropy	-.364	-.663	.366	
Mean	-.336	.135	.893	
Standard_Deviation	.325	-.132	-.871	
Smoothness	.105		.513	
RMS				.985
IDM				-.146

Extraction Method: Principal Component Analysis.  
Rotation Method: Varimax with Kaiser Normalization.

a. Rotation converged in 5 iterations.

**Figure 5.9:** Factor Analysis Output IV: Rotated Component Matrix

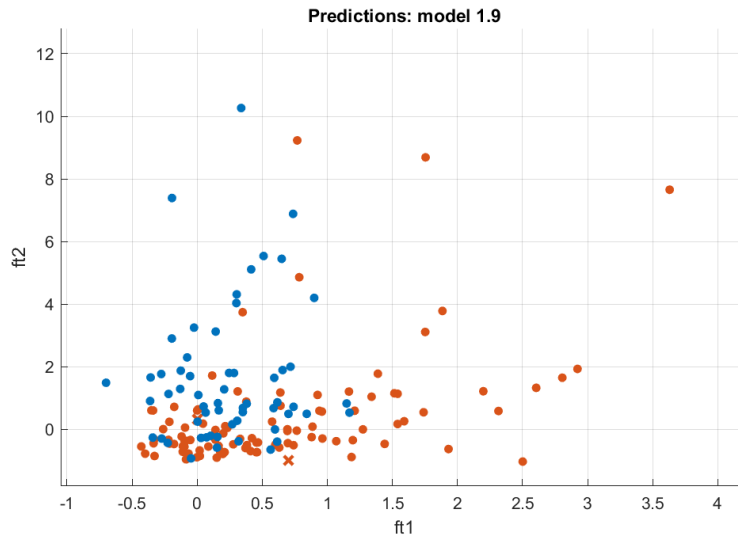


**Figure 5.10:** Scatter Plot of the Training Dataset

The area under the curve, or AUC, is calculated by taking the integral of the ROC curve, which displays the TPR values, with respect to FPR from FPR = 0 to FPR = 1. The AUC provides an overall evaluation of performance taking into account all of the thresholds. The AUC values can range anywhere from 0 to 1, with higher values suggesting a classifier that is better at its job. The 0.99 AUC that the current model possesses is evidence of the model's resiliency.

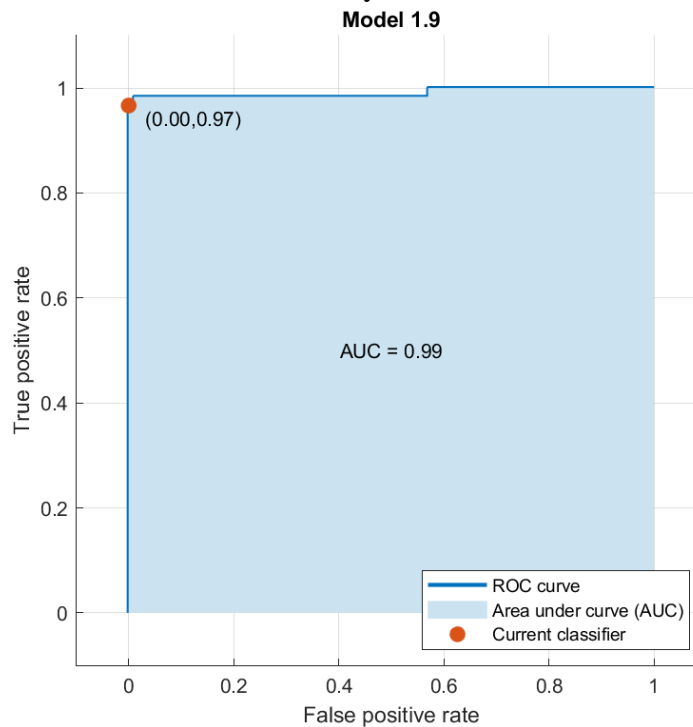


**Figure 5.11:** ROC Curve

Further investigation into the effectiveness of the proposed system is carried out with the use of a confusion matrix and a ROC curve. The cnn model and ROC curve that correspond to the features collected using specified attributes for classification at the sixth decomposition level are depicted in Figure 5.11. According to the area under the ROC curve, the level of the classifier's ability to correctly categorise pictures as either healthy or glaucomatous is 0.98. This level of competence can be seen in the ROC curve. The confusion matrix shows that the suggested technique mistakenly identifies just 2 images as typical instead of glaucoma and just 1 image as glaucoma instead of normal out of a total of 500 test shots. Using a classification models and a ROC curve, an additional investigation of the effectiveness of the system is carried out. On display are the confusion matrix and the ROC curve for such characteristics that were retrieved during the decomposition process using the specified classification features.

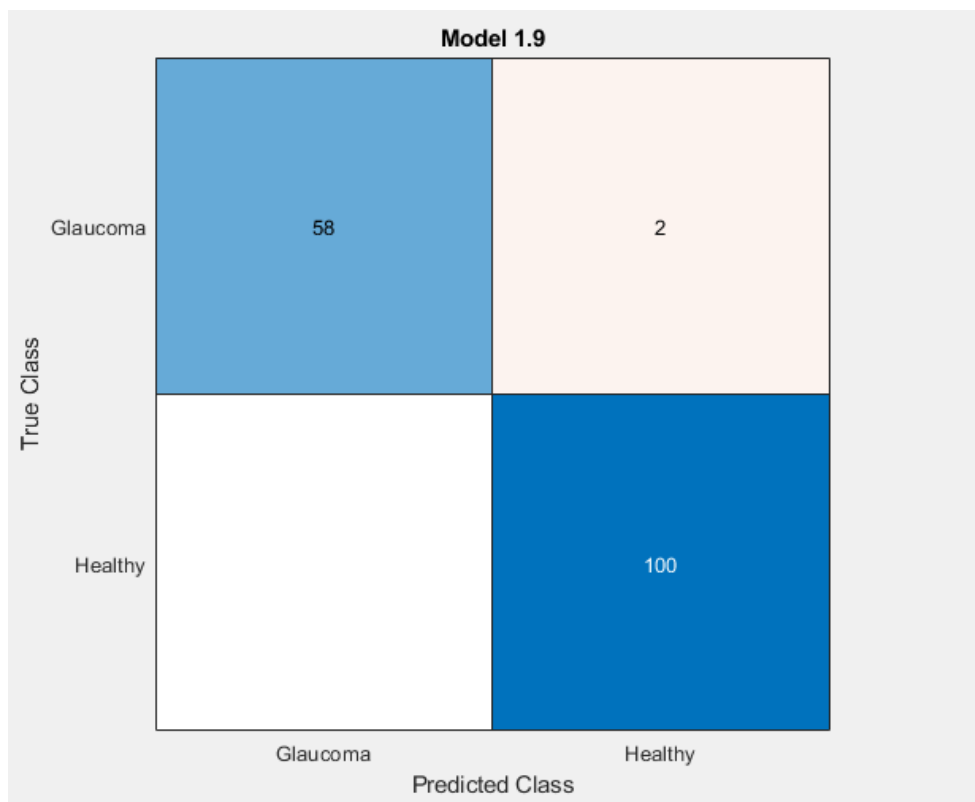


**Figure 5.12:** Confusion Matrix of SVM linear model

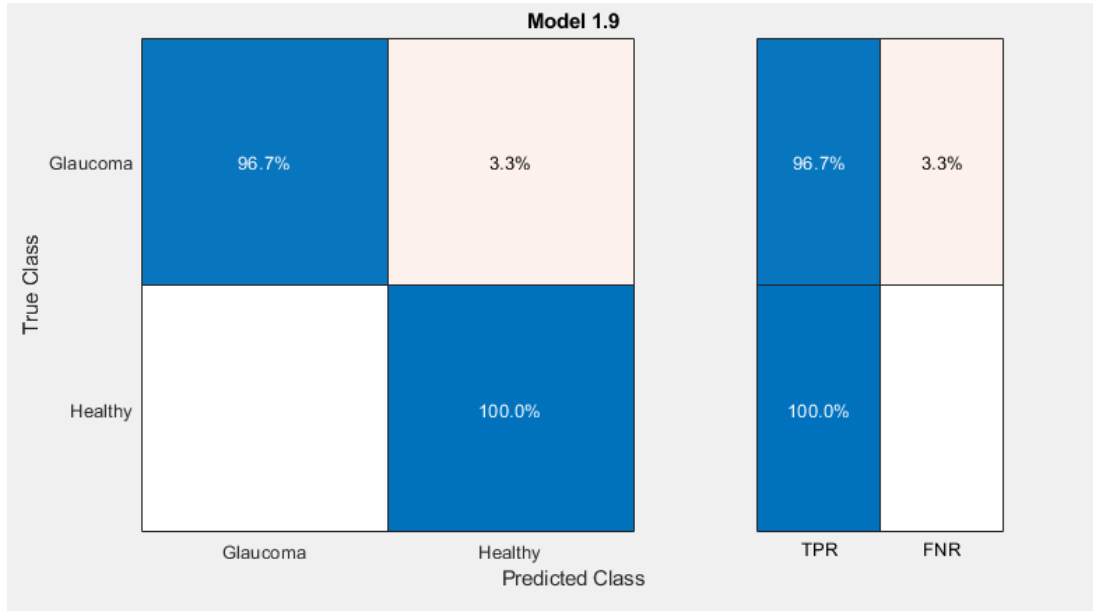


**Figure 5.13:** True Positive Results of SVM linear model

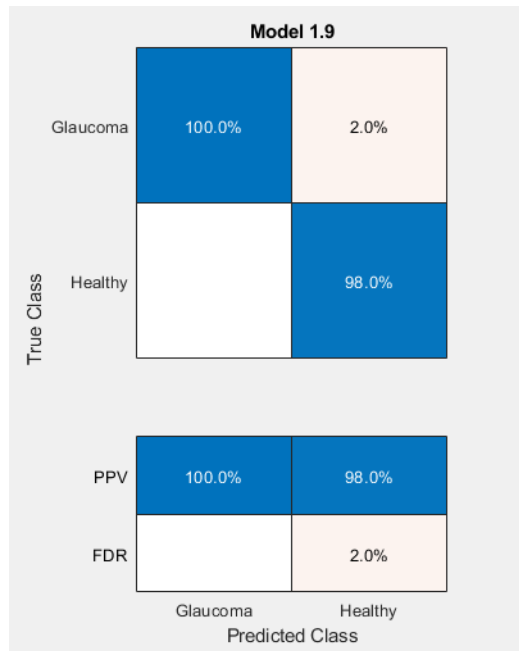


**Figure 5.14:** Positive Predicted Values of SVM linear model

Every point along the ROC curve denotes a unique combination of TPR and FPR values in a given value of the threshold. roc metrics considers all of the unique modified score threshold values that are associated with each class before generating a ROC curve for every class. After formulating a set of one-versus-all binary classifier questions, one for each class, roc metrics then derives the ROC curve for each class by resolving the related binary issue. This process is repeated for a multiclass problem. Every binary equation begins with the presumption that one class is positive as well as the other classes are negative. The system's dependability is once more brought into focus by the photographs, which exhibit very remarkable TPR and FNR values.

# CHAPTER 6: DISCUSSION & ANALYSIS

5.35 million OCT scans were conducted on the US Medicare population in 2014 alone, making OCT one of the most prevalent imaging procedures. The majority of recent studies have focused on the use of deep learning for glaucoma detection, avoiding cases that require identification beyond a non-specialist level interpretation and real-world scenarios, which include high myopes who are glaucoma suspects. Using a statistical method, the following part evaluated the performance of the created automated early glaucoma diagnosis framework. The robustness of the proposed technique was initially evaluated on OCT pictures and subsequently on fundus images as well. The proposed strategy merely employs a range of statistical features, including wavelet features such as mean, smoothness, and third moment, as well as neural network features gained through the factor analysis method's feature selection. Because each characteristic has a unique range, they are utilised in the proposed strategy. In this study, we assessed the efficacy of our proposed strategy by comparing its results to those of other approaches. The precision of our method is 95.24 percent. In this investigation, we applied fewer criteria than in prior studies; yet, the proposed technique correctly identified all normal classes and had greater accuracy than previous methods [18,21,24,27]. These findings provide evidence that glaucoma can be diagnosed using any one of the three statistical feature methodologies that were discussed. An inaccurate glaucoma quantification can occur when the disc centres in some myopic eyes are unable to be detected. This is especially true for eyes that have optic discs that are angled. The performance of the disc and fovea in their classification would not be affected in any way if it were unable to locate the centres of the disc and fovea since the method that we have described does not include disc centre identification. As a consequence of this, the method of machine learning that we proposed would be better able to differentiate between glaucoma sufferers and healthy individuals. To put it another way, the performance of our method for classifying images

is greater, despite the fact that it does not rely on image processing methods to automatically locate the disc's centre.

Glaucoma is an eye ailment that, if left untreated, destroys the nerve cells that aid in visual recognition. Excessive IOP enlarges the optic cup within the region of the optic disc, which is the primary cause of glaucoma's existence and progression, but it manifests in later phases of the diagnostic process. Cupping, as well as an increase in CDR and macula degradation, is a frequent finding in both clinical and automated glaucoma diagnostic techniques. The retina is damaged, resulting in a reduction in retinal thickness. Optical coherence tomography (OCT) and fundus imaging are utilised to assess the macula for glaucoma diagnosis. These two imaging technologies are particularly helpful for detecting and monitoring retinal tissue structures so that ocular diseases can be treated sooner. CCDR has been applied to fundus retinal imaging in the past by segmenting the optic cup and disc regions and then estimating their diameters. This study focuses on utilizing OCT to consistently measure macular thickness and then identifying the individual as glaucomatous or healthy. To extract the ILM, RPE, GCL, and other layers from OCT scans, a unique method is currently being developed. The proposed method then employed the layer's boundaries to determine the thickness of the overall layers, focusing on the Ganglion Cells Layer, which aids in the computation of the overall macular degeneration. The algorithm classifies the patient as either normal or glaucomatous based on the numbers generated. The proposed method is assessed utilizing a local dataset of 35 OCT pictures and the Kim Hospital Dataset, and the results demonstrate its validity.

In addition, the peripheral GCC in retinal GCC thickness maps is often narrower than the center GCC. This is seen in the diagram. In addition, as glaucoma advances, the thick GCC region changes from a circular shape to a distorted one. Because of this, it is an effective discriminator between healthy people and those with early glaucoma. As a result, the method utilised concepts that are generally utilised by medical professionals when glaucoma is being diagnosed. Recent studies have shown that damage to the macular security vulnerabilities zone is a more sensitive marker of early glaucoma than damage to the cpRNFL, and the results of the present investigation have shown that

macular pictures perform better than cpRNFL pictures do. This supports the findings of the previous studies. For the purpose of assessing classification performance, the region underneath the curves of the ROC was utilised (AUC). The AUC that can be achieved within the confines of this framework is... (19) Therefore, this technique ought to help to the advancement of glaucoma diagnostic criteria and uniformity.

When it comes to the treatment of glaucoma as well as research into the disease, medical professionals are required to consider the limitations of employing macular OCT. At first, it's possible that concomitant retinal illness and scan artefacts will make it difficult to analyse GCIPL using SD-OCT. The vast majority of the data that are currently available on macular OCT in glaucoma come from studies that exempted eyes with extra macular illness as well as those with poor photo quality, such as artefacts and lower signal intensity. This was done in order to ensure that the results were accurate and reliable. As a consequence of this, one ought to be prepared for larger variability in macular measures when dealing with real-world conditions. It is possible for the precise segmentation of the macular layers, which is necessary for the diagnosis and management of glaucoma patients, especially among the elderly, may be impeded by the presence of age-related macular disorders and drusen. The clinical staff has a responsibility to be aware of this issue and to take it into consideration. It is not possible to train algorithms to perform more effectively with the database of available OCT pictures. The study suffers from the problem of having a small number of participants, which may have reduced the statistically significant results of our results. In further studies, a greater number of myopic participants—both those with and without glaucoma—will need to be included in order to demonstrate that the proposed use of machine learning yields positive results.



# CHAPTER 7: CONCLUSION

This research concludes that macular optical coherence tomography (OCT) is an important imaging technique for glaucoma management and research. It provides information that is additional to the conventional diagnostic methods that glaucoma specialists use, notably in the analysis of patients who have early retinopathy and/or high myopia, as well as in the management of advanced illness. Macular optical coherence tomography (OCT) information is blended with data from statistical analysis to offer a more comprehensive understanding of the real nature of glaucoma progression. This was made possible by the invention and widespread application of AI methods in medicine.

From the tabulated findings, it is evident that the most effective method for detecting glaucoma is to use OCT image analysis. Due to glaucoma, the distortion in the cup region can be viewed more precisely in OCT pictures, which provide layer information of the retina (i.e. depth information of retinal). In conjunction with machine learning, the Wavelet Transform is utilised for feature extraction. Feature fusion-based techniques have demonstrated superior performance to those that utilize a single feature. Using small-scale image benchmarks, the manually generated features have demonstrated their effectiveness. The experimental results demonstrate that deep learning methods perform better than hand-crafted features. This integration provides an advanced platform for early glaucoma diagnosis as a result. Work is performed on all major elements, including structural (Macula) and functional characteristics. This will undoubtedly improve the quality of future medical care and research. The experimental results demonstrate that the proposed system outperforms and achieves a classification model accuracy of 95.24%. The presented approach also possesses a sensitivity of 91.794 percent and a specificity of 89.712 percent.



# CHAPTER 8: FUTURE WORK

Future work will involve the identification of precise location of macular layers and the incorporation of the layer's depth analysis with the statistical data retrieved and noted by ophthalmologists. It will make the system more robust and easier to categories. Future research can be conducted on OCT and fundus images to determine glaucoma types such as open angle, angle closure, etc. The segmentation and classification can be modified for improved outcomes.

Evaluating the deterioration of individual layers in an OCT image can make the detection of glaucoma more accurate. This can be accomplished by using the image. In addition, the validity of premature glaucoma detection can be strengthened by comparing the thicknesses of all retinal layers in normal eyes to the thickness of those in glaucoma eyes with the assistance of massive datasets. It seems like a possible research path in this industry would be to use deep learning methods to large-scale OCT photo benchmarks. The vast majority of studies have used their own own fundus and OCT image standards to evaluate their study; in contrast, there are very few photos benchmarks that are readily available to the public. For this purpose, it is vital to construct a large-scale image standard that is openly accessible to the general public for the purpose of evaluating future research. This will be helpful for identifying the greatest performance of additional investigation that will be evaluated on the very same data set, and it can lead to the establishment of effective CAD for the diagnosis of glaucoma.

# APPENDIX A

## Journal Paper Submission


Biomedical Signal Processing and Control  








HOME • LOGOUT • HELP • REGISTER • UPDATE MY INFORMATION • JOURNAL OVERVIEW  
MAIN MENU • CONTACT US • SUBMIT A MANUSCRIPT • INSTRUCTIONS FOR AUTHORS • POLICIES

Role: [author](#) Username: kainatali196


### ← Submissions Being Processed for Author

Page: 1 of 1 (1 total submissions)

Results per page 10 

Action 	Manuscript Number 	Title 	Initial Date Submitted 	Status Date 	Current Status 	
Action Links	BSPC-D-22-01979	Early detection of Glaucoma based on Wavelet Domain, Design of Experiment and Macular Layers using OCT Images	Jul 03, 2022	Jul 26, 2022	Decision in Process	

Page: 1 of 1 (1 total submissions)

Results per page 10 

# REFERENCES

- [1] A. Yildiz, "OCT in Glaucoma Diagnosis, Detection and Screening", in OCT - Applications in Ophthalmology. London, United Kingdom: IntechOpen, 2018 [Online]. Available: <https://www.intechopen.com/chapters/62200> doi: 10.5772/intechopen.78683
- [2] C S, Fathima and E N, Subhija, Glaucoma Detection Using Fundus Images and OCT Images (August 31, 2019). Government College of Engineering Kannur, International Conference on Systems, Energy & Environment (ICSEE) 2019. Available at SSRN: <https://ssrn.com/abstract=3445912> or <http://dx.doi.org/10.2139/ssrn.3445912>
- [3] Maetschke S, Antony B, Ishikawa H, Wollstein G, Schuman J, Garnavi R (2019) A feature agnostic approach for glaucoma detection in OCT volumes. PLoS ONE 14(7): e0219126.
- [4] Shabbir A, Rasheed A, Shehraz H, Saleem A, Zafar B, Sajid M, Ali N, Dar SH, Shehryar T. Detection of glaucoma using retinal fundus images: A comprehensive review. Math Biosci Eng. 2021 Mar 2;18(3):2033-2076. doi: 10.3934/mbe.2021106. PMID: 33892536.
- [5] [https://www.researchgate.net/publication/349720909\\_Detection\\_of\\_glaucoma\\_using\\_retinal\\_fundus\\_images\\_A\\_comprehensive\\_review](https://www.researchgate.net/publication/349720909_Detection_of_glaucoma_using_retinal_fundus_images_A_comprehensive_review)
- [6] Safaa Makram Mohamed et al 2020 J. Phys.: Conf. Ser. 1447 012010
- [7] Detry-Morel M. Facteurs de risque : la myopie [Is myopia a risk factor for glaucoma?]. J Fr Ophtalmol. 2011 Jun;34(6):392-5. French. doi: 10.1016/j.jfo.2011.03.009. Epub 2011 Jun 1. PMID: 21632150.
- [8] <https://www.mayoclinic.org/diseases-conditions/glaucoma/symptoms-causes/syc-20372839>
- [9] B. Gupta, M. Tiwari, S. S. Lamba, Visibility improvement and mass segmentation of mammogram images using quantile separated histogram equalisation with local contrast enhancement, CAAI Trans. Intell. Technol., 4 (2019), 73–79.

- [10] S. Maheshwari, V. Kanhangad, R. B. Pachori, S. V. Bhandary, U. R. Acharya, Automated glaucoma diagnosis using bit-plane slicing and local binary pattern techniques, *Comput. Biol. Med.*, 105 (2019), 72–80.
- [11] Kansal V, Armstrong JJ, Pintwala R, Hutnik C (2018) Optical coherence tomography for glaucoma diagnosis: An evidence based metaanalysis. *PLoS ONE* 13(1): e019062
- [12] Sharma P, Sample PA, Zangwill LM, Schuman JS.
- [13] Stein JD, Talwar N, LaVerne AM, Nan B, Lichter PR. Trends in use of ancillary glaucoma tests for patients with open-angle glaucoma from 2001 to 2009. *Ophthalmology*. 2012;119:748–758. [PMC free article] [PubMed] [Google Scholar]
- [14] Sharma P, Sample PA, Zangwill LM, Schuman JS.
- [15] Kamalipour, Alireza, and Sasan Moghimi. “Macular Optical Coherence Tomography Imaging in Glaucoma.” *Journal of ophthalmic & vision research* vol. 16,3 478-489. 29 Jul. 2021, doi:10.18502/jovr.v16i3.9442
- [16] Odaibo SG. Re: Phene et al.: Deep learning and glaucoma specialists: the relative importance of optic disc features to predict glaucoma referral in fundus photographs (*Ophthalmology*. 2019;126:1627-1639). *Ophthalmology*. 2020 Aug;127(8):e57-e58. doi: 10.1016/j.ophtha.2020.03.041. PMID: 32703394.
- [17] <https://www.sciencedirect.com/topics/medicine-and-dentistry/fundus-imaging>
- [18] Medeiros FA, Zangwill LM, Bowd C, Vessani RM, Susanna R Jr, Weinreb RN. Evaluation of retinal nerve fiber layer, optic nerve head, and macular thickness measurements for glaucoma detection using optical coherence tomography. *American Journal of Ophthalmology*. 2005;139:44-55
- [19] Park SB, Sung KR, Kang SY, Kim KR, Kook MS. Comparison of glaucoma diagnostic capabilities of Cirrus HD and stratus optical coherence tomography. *Archives of Ophthalmology*. 2009;127:1603-1609
- [20] Fercher AF, Drexler W, Hitzenberger CK, Lasser T. Optical coherence tomography-principles and applications. *Rep Progr Phys* 2003;66:239.
- [21] Abramoff MD, Garvin MK, Sonka M. Retinal imaging and image analysis. *IEEE Rev Biomed Eng* 2010;3:169–208.

- [22] Leung CK. Diagnosing glaucoma progression with optical coherence tomography. *Curr Opin Ophthalmol.* 2014 Mar;25(2):104-11. doi: 10.1097/ICU.0000000000000024. PMID: 24370973.
- [23] Yang X., Hamaguchi S., Sun Y., Xiao S. "Detect of optic disk centre based on Gaussian vessel detector and tangent information transform" *IEEE 2011, 4th international conference on biomedical engineering and informatics (BMEI), Vol.1, pp 250-254, October 2011.*
- [24] Dua S., Acharya U.R., Chowriappa P., Sree S.V., "Wavelet based energy features for glaucomatous image classification" *IEEE transaction on information technology in biomedicine, Vol. 16, no.1, pp 80-87, January 2012.*
- [25] Nithya, K. (2016). Screening of Diabetic Patients attending Diabetology Out Patient Department for Primary Open Angle Glaucoma (Doctoral dissertation, Coimbatore Medical College, Coimbatore).
- [26] Aquino A., Gegundez-Arias M.E, Marin D. "Detecting the optic disk boundary in digital fundus images using morphological, edge detection and feature extraction techniques" *IEEE transactions on medical imaging, Vol.29, pp1860-1869, November 2010*
- [27] Wong wing kee Damon, Jimmy Liu, Tan Ngan Meng, Yin fengshou, Wong Tien Yin "Automatic detection of optic cup using vessel kinking in digital retinal fundus images", *IEEE, ISBI 2012, pp 1647-1650, May 2012*
- [28] A. Agarwal, S. Gulia, S. Chaudhary, M. K. Dutta, R. Burget and K. Riha, "Automatic glaucoma detection using adaptive threshold based technique in fundus image," *2015 38th International Conference on Telecommunications and Signal Processing (TSP), 2015, pp. 416-420, doi: 10.1109/TSP.2015.7296295.*
- [29] J. Carrillo, L. Bautista, J. Villamizar, J. Rueda, M. Sanchez, D. Rueda, Glaucoma detection using fundus images of the eye, *2019 XXII Symposium on Image, Signal Processing and Artificial Vision (STSIVA), IEEE, 2019, 1-4.*
- [30] Qi Y, Reisman CA, Wang Z, Fukuma Y, Hangai M, Yoshimura N, Tomidokoro A, Araie M, Raza AS, Hood DC, Chan K. Automated layer segmentation of macular OCT images using dual scale gradient information. *Optics Express.* 2010; 18(20):21293-307.

- [31] Qi Y, Reisman CA, Wang Z, Fukuma Y, Hangai M, Yoshimura N, Tomidokoro A, Araie M, Raza AS, Hood DC, Chan K. Automated layer segmentation of macular OCT images using dual scale gradient information. *Optics Express*. 2010; 18(20):21293–307.
- [32] Kim, Y. K., Jeoung, J. W., & Park, K. H. (2017). Inferior Macular Damage in Glaucoma: Its Relationship to Retinal Nerve Fiber Layer Defect in Macular Vulnerability Zone. *Journal of Glaucoma*, 26(2), 126-132. <https://doi.org/10.1097/IJG.0000000000000576>
- [33] [https://www.researchgate.net/publication/49823500\\_Spectral-domain\\_optical\\_coherence\\_tomography\\_for\\_the\\_diagnosis\\_and\\_follow-up\\_of\\_glaucoma](https://www.researchgate.net/publication/49823500_Spectral-domain_optical_coherence_tomography_for_the_diagnosis_and_follow-up_of_glaucoma)
- [34] Sehi M, Grewal DS, Sheets CW, Greenfield DS. Diagnostic ability of Fourier-domain vs time-domain optical coherence tomography for glaucoma detection. *Am J Ophthalmol*. 2009 Oct;148(4):597-605. doi: 10.1016/j.ajo.2009.05.030. Epub 2009 Jul 9. PMID: 19589493; PMCID: PMC2784699.
- [35] H. Yamada, T. Akagi, H. Nakanishi, H. O. Ikeda, Y. Kimura, K. Suda, et al., Microstructure of peripapillary atrophy and subsequent visual field progression in treated primary open-angle glaucoma, *Ophthalmology*, 123 (2016), 542–551.
- [36] J. B. Jonas, Clinical implications of peripapillary atrophy in glaucoma, *Curr. Opin. Ophthalmol.*, 16 (2005), 84–88.
- [37] K. H. Park, G. Tomita, S. Y. Liou, Y. Kitazawa, Correlation between peripapillary atrophy and optic nerve damage in normal-tension glaucoma, *Ophthalmol.*, 103 (1996), 1899–1906.
- [38] Chauhan BC, Burgoyne CF. From clinical examination of the optic disc to clinical assessment of the optic nerve head: a paradigm change. *Am J Ophthalmol*. 2013;156(2):218–27.
- [39] Chen TC. Spectral domain optical coherence tomography in glaucoma: qualitative and quantitative analysis of the optic nerve head and retinal nerve fiber layer (an AOS thesis). *Trans Am Ophthalmol Soc*. 2009;107: 254–81.
- [40] Chauhan BC, O'Leary N, AlMobarak FA, Reis ASC, Yang H, Sharpe GP, Hutchison DM, Nicoleta MT, Burgoyne CF. Enhanced detection of openangle

- glaucoma with an anatomically accurate optical coherence tomography-derived neuroretinal rim parameter. *Ophthalmology*. 2013; 120(3):535–43.
- [41] Kausu, T. R., Gopi, V. P., Wahid, K. A., Doma, W., & Niwas, S. I. (2018). Combination of clinical and multiresolution features for glaucoma detection and its classification using fundus images. *Biocybernetics and Biomedical Engineering*, 38(2), 329-341.
- [42] Bambo, M. P., Ferrandez, B., Güerri, N., Fuertes, I., Cameo, B., Polo, V., ... & Garcia-Martin, E. (2016). Evaluation of contrast sensitivity, chromatic vision, and reading ability in patients with primary open angle glaucoma. *Journal of ophthalmology*, 2016.
- [43] Nithya, K. (2016). Screening of Diabetic Patients attending Diabetology Out Patient Department for Primary Open Angle Glaucoma (Doctoral dissertation, Coimbatore Medical College, Coimbatore).
- [44] Agarwal, A., Gulia, S., Chaudhary, S., Dutta, M. K., Burget, R., & Riha, K. (2015, July). Automatic glaucoma detection using adaptive threshold based technique in fundus image. In *2015 38th International Conference on Telecommunications and Signal Processing (TSP)* (pp. 416-420). IEEE.
- [45] Cheng, J., Liu, J., Xu, Y., Yin, F., Wong, D. W. K., Tan, N. M., ... & Wong, T. Y. (2013). Superpixel classification based optic disc and optic cup segmentation for glaucoma screening. *IEEE transactions on medical imaging*, 32(6), 1019-1032.
- [46] An, G., Omodaka, K., Hashimoto, K., Tsuda, S., Shiga, Y., Takada, N., ... & Nakazawa, T. (2019). Glaucoma diagnosis with machine learning based on optical coherence tomography and color fundus images. *Journal of healthcare engineering*, 2019.
- [47] Septiarini, A., & Harjoko, A. (2015). AUTOMATIC GLAUCOMA DETECTION BASED ON THE TYPE OF FEATURES USED: A REVIEW. *Journal of Theoretical & Applied Information Technology*, 72(3).
- [48] Kirar, B. S., & Agrawal, D. K. (2019). Computer aided diagnosis of glaucoma using discrete and empirical wavelet transform from fundus images. *IET Image Processing*, 13(1), 73-82.



- [49] Nirmala, K., Venkateswaran, N., & Kumar, C. V. (2017, November). HoG based Naive Bayes classifier for glaucoma detection. In TENCON 2017-2017 IEEE Region 10 Conference (pp. 2331-2336). IEEE.
- [50] Wu, J. H., Nishida, T., Weinreb, R. N., & Lin, J. W. (2021). Performances of machine learning in detecting glaucoma using fundus and retinal optical coherence tomography images: A meta-analysis. *American Journal of Ophthalmology*.
- [51] Pal, A., Moorthy, M. R., & Shahina, A. (2018, October). G-eyenet: A convolutional autoencoding classifier framework for the detection of glaucoma from retinal fundus images. In 2018 25th IEEE international conference on image processing (ICIP) (pp. 2775-2779). IEEE.
- [52] Tjandrasa, H., Wijayanti, A., & Suciati, N. (2012). Optic nerve head segmentation using hough transform and active contours. *TELKOMNIKA Indonesian Journal of Electrical Engineering*, 10(3), 531-536.
- [53] Raja, H., Akram, M. U., Hassan, T., Ramzan, A., Aziz, A., & Raja, H. (2022). Glaucoma Detection Using Optical Coherence Tomography Images: A Systematic Review of Clinical and Automated Studies. *IETE Journal of Research*, 1-21.
- [54] Chen, X., Xu, Y., Yan, S., Wong, D. W. K., Wong, T. Y., & Liu, J. (2015, October). Automatic feature learning for glaucoma detection based on deep learning. In *International conference on medical image computing and computer-assisted intervention* (pp. 669-677). Springer, Cham.
- [55] Hagiwara, Y., Koh, J. E. W., Tan, J. H., Bhandary, S. V., Laude, A., Ciaccio, E. J., ... & Acharya, U. R. (2018). Computer-aided diagnosis of glaucoma using fundus images: A review. *Computer methods and programs in biomedicine*, 165, 1-12.
- [56] Gupta, G. (2011). Algorithm for image processing using improved median filter and comparison of mean, median and improved median filter. *International Journal of Soft Computing and Engineering (IJSCE)*, 1(5), 304-311.
- [57] Ma, & Liu, & Ren, & Luo, Yu-Feng. (2019). Detection of Collapsed Buildings in Post-Earthquake Remote Sensing Images Based on the Improved YOLOv3. *Remote Sensing*. 12. 44. 10.3390/rs12010044.

- [58] John, G. H., Kohavi, R., & Pflieger, K. (1994). Irrelevant features and the subset selection problem. In *Machine learning proceedings 1994* (pp. 121-129). Morgan Kaufmann.
- [59] Kafieh, R., Rabbani, H., & Kermani, S. (2013). A review of algorithms for segmentation of optical coherence tomography from retina. *Journal of medical signals and sensors*, 3(1), 45.

# COMPLETION CERTIFICATE

It is certified that the thesis titled “**Early Detection of Glaucoma based on Wavelet Domain and Design of Experiment using OCT Images**” submitted by CMS ID. 00000275584, NS Kainat Ali of MS-2018 Mechatronics Engineering is completed in all respects as per the requirements of Main Office, NUST (Exam branch).

Supervisor: \_\_\_\_\_

Dr. Mohsin Islam Tiwana

Date: \_\_\_\_\_